XPS STUDIES OF ADHESION AT ORGANOSILANE/ALUMINUM INTERFACES

by

YIN-LING LEUNG

B.Sc., National Taiwan Normal University, 1988

A THESIS SUBMITTED IN PARTIAL FULFILLMENT OF

THE REQUIREMENTS FOR THE DEGREE OF

MASTER OF SCIENCE

in

THE FACULTY OF GRADUATE STUDIES

DEPARTMENT OF CHEMISTRY

We accept this as conforming

to the required standard

THE UNIVERSITY OF BRITISH COLUMBIA

August 1992

In presenting this thesis in partial fulfilment of the requirements for an advanced degree at the University of British Columbia, I agree that the Library shall make it freely available for reference and study. I further agree that permission for extensive copying of this thesis for scholarly purposes may be granted by the head of my department or by his or her representatives. It is understood that copying or publication of this thesis for financial gain shall not be allowed without my written permission.

Department of CHEMISTRY

The University of British Columbia
Vancouver, Canada

Date Sept. 28, 1992

Abstract

The work in this thesis deals with silane to aluminum adhesion. Angular dependent X-ray photoelectron spectroscopy (ADXPS) with the bias potential technique is used for the first time to probe silane/aluminum interfaces, the investigation aims to find evidence of direct chemical bonding between the two materials.

7074-T6 aluminum alloy panels are subjected to two surface pretreatments: degreasing treatment and chemical etching treatment which affect exposure of the Al oxide above the metal. Uppermost, though, is a carbon layer. ADXPS measurements show that the surfaces formed from these two treatments have different morphologies: one has continuous carbon and the other has carbon in patchy form. These different morphologies give different behavior in the adhesion. The organosilanes γ-glycidoxy-propyltrimethoxysilane (γ-GPS), γ-aminopropyltrimethoxysilane (γ-APS), and γ-mercaptopropyltrimethoxysilane (γ-MGPS) were deposited on to the Al panels, and ADXPS was used to characterize the interfaces, as well as the orientations of the organofunctional groups.

The combination of ADXPS and the new negative biasing potential technique, proposed by Pertsin and Pashunin, showed the presence of an extra peak in the Al_{2p} spectra for γ-GPS and γ-MGPS deposited on to chemically etched aluminum. This extra structure may indicate that direct Al-O-Si bonding occurs between these silanes and the aluminum oxide. No significant change for the Al_{2p} peak is found when γ-GPS is deposited on degreased aluminum. That indicates that the continuous carbonaceous overlayer limits the interaction between the silane and the degreased aluminum, while the patchy carbonaceous overlayer provides some carbon-free aluminum oxide for

interaction with the silane. By contrast, γ-APS shows no evidence for direct chemical bonding with aluminum in either acidic medium (pH=3.0) or alkaline medium (pH=10.4). The structures of the γ-APS films deduced from the ADXPS measurements explain this aspect: in both these cases the ≡Si-OH ends cannot approach the Al-OH groups on the metal surface, so no direct interaction takes place.

Table of Contents

List of Tables

List of Figures

Acknowledgements

I would like to thank my supervisor, Professor K.A.R. Mitchell, for sponsoring this work and for his advice and comments on this thesis. I am especially grateful to Dr. P.C. Wong, Professor M.Y. Zhou, and Professor Y.P. Yang for helping with the XPS measurements, and giving me many helpful discussions. I also acknowledge the efforts of the Departmental workshop staff in keeping the equipment in working order for this research, and the financial support provided by the Defence Research Establishment Pacific.

Finally, I thank to my family and my friends for their encouragement in these two years.

Chapter 1. Introduction

"When a plate of gold shall be bonded with a plate of silver or joined thereto, it is necessary to beware of three things, of dust, of wind and of moisture: for if any come between the gold and silver they may not be jointed together . . . "

De Proprietatibus Rerum (The Properties of Things) . . . . 1250 AD[1.1]

A. General

The application of adhesion has a long history in human life. Do we exactly know how things stick together? Can things be bonded together forever? How can some very different types of materials adhere together? Surprisingly, there have been more questions than solutions about adhesion phenomena. Several theories have been developed for the sake of understanding their mechanisms, nevertheless, the overall picture is still not complete (fundamentals of adhesion can be found in references 1.2 and 1.3).

The adhesion of organic polymer to metal is widely employed in industry. To afford protection or decoration, polymers must adhere to substrates and remain adhered during the service environment. For promoting adhesion between these two incompatible surfaces, appropriate surface modifications are needed. Commonly, surface pretreatments [1.4] are performed to roughen the adherends and to remove their weak boundary layer. Also, adhesion promoters or coupling agents [1.5, 1.6], which may form primary bonds either with the substrates or polymeric coatings, or both, are usually applied between the adherends to improve the bond resistance across the interface. Organosilanes [1.7, 1.8], for instance, are considered as effective coupling agents; their

bifunctional nature provides a hybrid linkage between organic resins and metal substrates. Covalent bond formation is particularly popular in explaining the coupling function of silanes.

Figure 1.1 schematically indicates the interfacial region [1.9] in a polymer/metal joint. It is believed that this region has unique properties and plays a key role in determining the goodness of the adhesion. For example, poorly durable bondings are often a consequence of poor interfacial properties. Measuring and understanding the characteristics of this region enables one to get insight into adhesion phenomena. Thus, investigating the interfacial region becomes one of the frontier areas in today's adhesion science.

Various surface analysis techniques have been used to study polymer/metal adhesion. Of all the presently available surface analysis instruments, X-ray photoelectron spectroscopy (XPS) is generally more quantitative, more interpretable and more informative with regard to chemical information. Cross sections are low for H and He, but in principle XPS is applicable to all elements. The usage of soft X-ray sources performs a non-destructive surface analysis. By quantitative and qualitative measurements, elemental composition and chemical bonding information can be obtained, while the angle dependent measurement (ADXPS) generates depth profiling without ruining the sample surface.

In summary, this thesis aims to give a view of how XPS provides information on surface and interface chemistry for silane/aluminum adhesions. At the beginning, this chapter gives a description of silane coupling agents including their life history and their adsorption mechanisms on mineral surfaces. Then, literature about the silane/metal bond

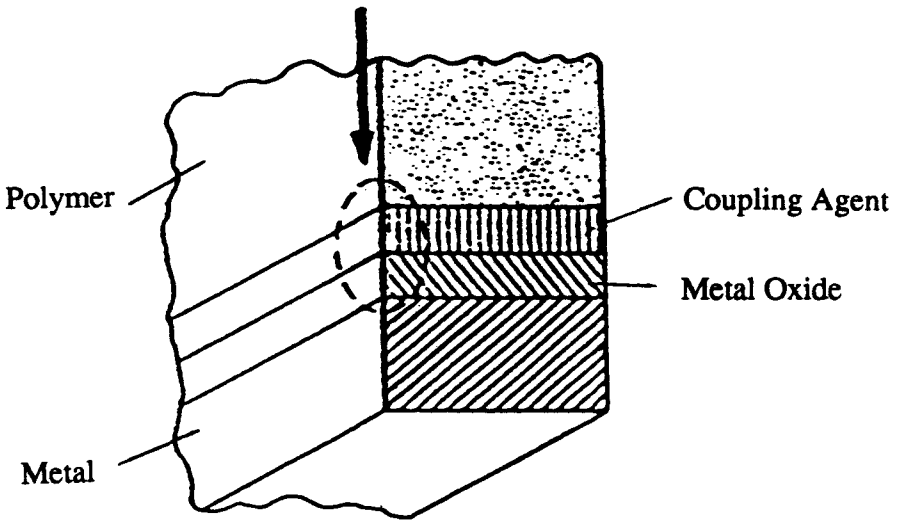

Figure 1.1 A typical complex adhesive bond. Note that the interfacial region [1.10] is the volume of material slightly below the surface of the metal and extending into the polymer, while interface is the boundary between two phases.

formation studies are reviewed. General concepts of polymer/metal interface analysis, along with the bias potential technique are given, as well as the objectives of our study.

In the second chapter, we focus on the basic principles of XPS, specifically to identify what enables it to perform as a surface analytical technique. Based upon the MAX 200 system used in this work, the main components of a XPS spectrometer are introduced as well. The third chapter discusses the results obtained in our silane/ aluminum interfaces studies. The final chapter includes some concluding remarks, as well as suggestions for further research.

B. Silane Coupling Agents

> *"It is not possible for two things to be fairly united without a third, for they need a bond between them which shall join them both, that as the first is to the middle, so is the middle to the last, then since the middle becomes the first and the last, and the last and the first become middle, of necessity, all will come to be the same, and being the same with one another, all will be a unity."*
>
> *Plato, Timaeus [1.11]*

B-1. Historical

When glass fibres were first used to reinforce organic resins in the 1940s' [1.12], scientists tried to find a third material for adhering these two extremely different materials together. Organofunctional silanes, with organic and inorganic dual properties,

were recognized to operate as effective coupling agents. Probably amino-functional silanes were the first developed coupling agents [1.6]. They were specially designed to overcome the poor adhesion of phenolic resin to glass fibre composites. Afterwards, methacrylate functional silanes were rapidly developed in the field of glass-fibre reinforced polyester composites [1.6].

From the 1960s to early 1970s, effort was spent on the theory and practice of silane chemistry and technology [1.13]. Pleuddemann and his coworkers evaluated over a hundred different silanes in glass reinforced polyester and epoxy composites. Studies of coupling mechanisms enabled them to discuss the merits of several different adhesion theories [1.13]. During the mid-1960s, the disastrous effect of water on the bond strength of adhesives [1.14] and surface coatings [1.15] encouraged the study of coupling agents to mitigate this effect.

In 1981, it was first reported that some polymeric silane mixtures [1.16] acted as effective corrosion inhibitors and releasing agents for metal substrates. Afterwards, investigators became interested in formulating different silanes with other anti-corrosion agents to develop new and effective primers.

B-2. Adsorption on Metal Surfaces

All silane coupling agents have the general formula $X_3Si(CH_2)_nY$, where X is a hydrolyzable group on silicon, Y is an organofunctional group selected for compatibility with organic polymers, and n can vary from 0 to 3. Several commercially available

silanes with an indication of their functional groups, chemical structures and common abbreviations are given in Table 1.1 [1.17].

Numerous studies have been reported regarding mechanisms that may explain how and why silanes generally lead to adhesion improvement. It is commonly accepted that silanes hydrolyze initially stepwise in aqueous solution (Figure 1.2a) to silanetriol which may condense to oligomeric siloxanols or be adsorbed on the metal surface [1.18, 1.19]. On metal surfaces, water is adsorbed as hydroxyl groups (M-OH) and as molecular water held by hydrogen bonding to the surface [1.20]. These M-OH groups hydrogen bond with the generated silanetriol or oligomers (Figure 1.2b) and consequently, a covalent linkage of M-O-Si is formed in the interface after eliminating a water molecule (Figure 1.2c). The remaining silanol group may condense with the adjacent silanol to form polysiloxane or remain partly uncondensed at the surface. The composition of the silane film is nonuniform [1.21, 1.22]. It may contain a strongly held polysiloxane net-work and small siloxane molecules or some uncondensed silanols.

B-3. Literature Review

The nature of adsorbed silane films on glass, silica, and mica [1.23, 1.24] and metal substrates, such as iron or aluminum [1.25-1.28], has been studied by numerous investigators. Most effort was used to get evidence that covalent bonds actually exist and are responsible for the improved performance. There is a number of indirect evidence supporting the theory of surface bonds, however, the direct evidence is very limited.

Table 1.1 Representative commercial silanes [1.17]

Organofunctional group	Structural Formula	Abbreviation
1. Vinyl	$CH_2=CHSi(OCH_3)_3$	VS
2. Chloropropyl	$Cl(CH_2)_3Si(OCH_3)_3$	CPS
3. Epoxy	$CH_2\overset{O}{\diagdown\diagup}CHCH_2O(CH_2)_3(OCH_3)_3$	GPS
4. Methacrylate	$CH_2=\overset{CH_3}{\overset{\vert}{C}}-COO(CH_2)_3Si(OCH_3)_3$	MPS
5. Primary amine	$H_2N(CH_2)_3Si(OCH_3)_3$	APS
6. Mercapto	$HS(CH_2)_3Si(OCH_3)_3$	MGPS

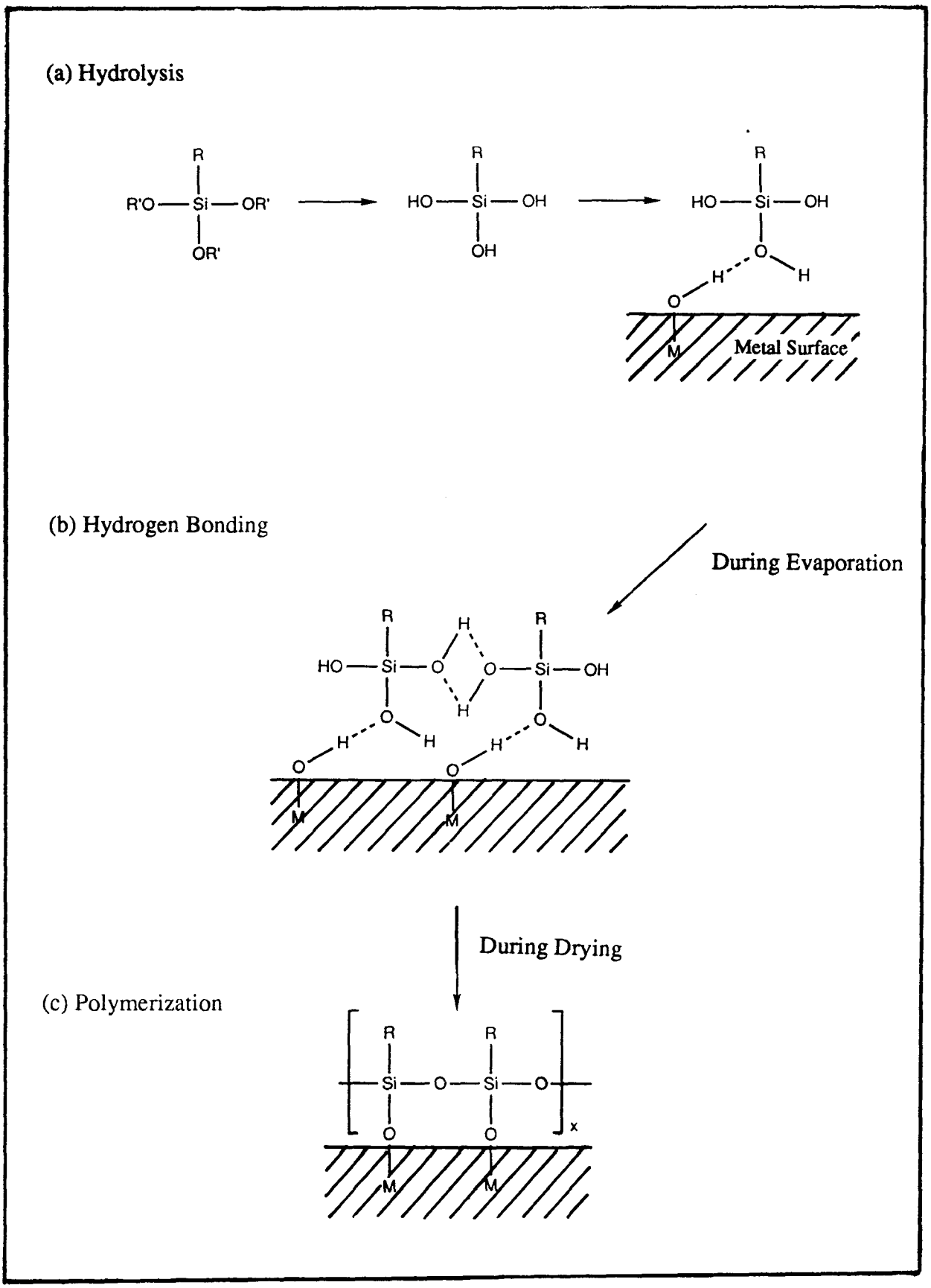

Figure 1.2 Deposition of silane on metal surface

Gettings et al. [1.25] probed γ-glycidoxypropyltrimethoxysilane (γ-GPS)/steel and γ-aminopropyltriethoxysilane (γ-APES)/steel interfaces with static secondary ion mass spectrometry (SSIMS) and XPS. A secondary ion of mass 100, assigned as $FeSiO^+$, was detected in the former case. They suggested that this was strong evidence for the formation of direct Fe-O-Si chemical bonding between γ-GPS and mild steel. However, it has also been recognized that secondary ions generated in SSIMS could be formed by incident-beam bombardment effects [1.29].

Vibrational spectroscopy such as infrared (IR) spectroscopy has frequently been used to examine silane/metal interfaces. Allen et al. [1.28] investigated γ-GPS and Al alloy interfaces, and suggested that the hydroxyl adsorption band around 3400 cm^{-1} was due to hydrogen bonding (H-bonding) between the silanols and Al. Boerio and coworkers extensively studied the deposition of γ-APES and γ-GPS on different metals such as iron, aluminum, and titanium [1.26, 1.27]. Using IR in combination with Auger electron spectroscopy (AES) and XPS, they concluded γ-GPS did not interact strongly with the oxide layer on 2024 Al alloy. For the deposition of γ-APES, on the evidence of the Auger band, they suggested amino groups coordinated with Cu(I) ions (one of the minor components in 2024 Al alloy), whilst the IR absorption band near 1080 cm^{-1} was related to the formation of an aluminosiloxane polymer. Recently, inelastic electron tunneling spectroscopy (IETS) [1.30-1.32] has been used to investigate the interaction between silanes and aluminum, but in none of these reports could an interfacial bond be detected.

Matienzo et al. [1.33] evaluated the resistance of polymer/7075-T6 Al joints against hydration and Cl^- corrosion. Several coupling silanes were used in the modification of Al panels. They found that of the most commonly employed adhesion

promoters, γ-aminopropyltrimethoxysilane (γ-APS) performed the worst, while γ-mercaptopropyltrimethoxysilane (γ-MGPS) had the most outstanding performance and γ-GPS ranked between them. In corrosion studies of polymer/2024 Al adhesion, Theidman et al. [1.34] believed that the durability of the bonding depended on the nature of materials as well as the acidity of the silane solutions. Boerio and Williams [1.26], studied the adsorption of γ-APES on iron mirrors. By investigating the hydrothermal stability of iron-epoxy lap joints, they found γ-APES has a better performance at pH=8.0 than at pH=12. They concluded two different molecular structures of γ-APES films in acidic and alkaline media [1.26]. However, they lacked direct evidence in support from the IR absorption bands.

Most investigators have their own views on the bonding between silanes and metal surfaces. Thus, it is necessary to distinguish whether conclusions are based on direct evidence or deductive reasoning.

C. Surface Analysis - Polymer/Metal Adhesion

C-1. General Concepts

Fundamental study of polymer/metal adhesion involves characterizing the interface, and developing mechanistic insight into the factors responsible for the bonding and durability. Which is the best surface analysis technique for polymer/metal interface study? In fact, it depends on which aspect being studied. Baun [1.9] categorized fifty-four surface characterization methods useful in analyzing six aspects of adhesion. Good summaries of the four major surface analytical techniques, namely XPS, AES, ISS, and

SIMS are given by Hofmann [1.35]. Table 1.2 summarizes their characteristics in surface analysis.

It is necessary to point out that those surfaces involved in applied science are more complex than those in single-crystal surface science. Surface characterization is seldom complete for real surfaces, and is at best simply adequate for the purpose; usually depth profiling (by destructive ion sputtering or angular dependent measurement) is needed for a buried interface. Even a "real surface" analysis must be performed under ultrahigh vacuum (UHV) conditions (10^{-9} torr or less), since even small amounts of residual gas in the analysis chamber can contaminate the sample surface and affect a measurement.

A common phenomenon is sample charging, which frequently happens in the polymer/metal interface analysis. For example, in a XPS analysis, the emission of photoelectrons from a solid can leave a residual positive charge on the sample surface. If the sample is a conductor, and is in good contact with the spectrometer, these charges can be quickly neutralized by electrons flowing from the grounded sample holder. For a poor conductor or an insulator, however, charge neutralization may be incomplete, and the established positive potential may retard the outgoing electrons. As a result, the surface exhibits charging. If the charging process is uniform, the spectrum simply shifts by a constant amount determined by the surface potential of the sample. However, the properties of some surface areas will not be identical; different regions may emit photoelectrons at different rates, thereby leading to an uneven charge distribution (i.e. differential charging). Care is needed in data interpretation that the effects of these charges in a XPS spectrum are not mistaken for chemical shifts.

Table 1.2 Some surface techniques and their characteristics [1.35]

Technique		Acronym	Probe Particle	Measured Particle	*Basic Information
1. Auger Electron Spectroscopy	[1.36]	AES	electron	electron	E, D_d, D_{nd}
2. Ion Scattering Spectroscopy	[1.37]	ISS	ion	ion	E
3. Secondary Ion Mass Spectroscopy	[1.29]	SIMS	ion	ion	E, C, D_d
4. X-ray Photo-electron Spectroscopy	[1.36]	XPS	photon	electron	E, C, D_d, D_{nd}

* E : Elemental Analysis
C : Chemical Analysis
D_d : Destructive Depth Profile
D_{nd} : Nondestructive Depth Profile

C-2. Bias Potential Technique

The charging effect is most often an unwanted phenomenon in surface analysis. However, Pertsin and Pashunin [1.38] have recently shown that the application of a negative potential to a sample during XPS study can help to reveal chemical information specifically for interfaces between a thin film of insulator on a conductor. Figure 1.3 shows a particular case for a thin polymer/metal interface. ΔS is a small element on the polymer surface. The steady-state potential, φ_s, of ΔS is determined by the currents i_1, i_2, and i_3. They are respectively: the electron current emitted from ΔS, the current striking the sample surface from vacuum, and the current between ΔS and the spectrometer via the sample holder.

Assuming Ohm's law, i_3 relates to φ_s and the sample holder potential, φ_h, as

$$i_3 = c\,(\varphi_s - \varphi_h) \qquad (1.1)$$

where c is the electrical conductivity between ΔS and the sample holder.

During a XPS analysis, the surface gradually develops a positive potential φ_s, which will attract stray electrons to the surface. This implies that i_2 is a function of φ_s; i_2 should tend to saturation with increasing φ_s and become zero for negative φ_s. If the variation of φ_s is not large, Pertsin and Pashunin proposed that i_2 is also governed by the electron withdrawing of ΔS, c'. That is, the behavior of i_2 may be approximated by

$$i_2 = i_2(0) + c'\varphi_s \qquad (1.2)$$

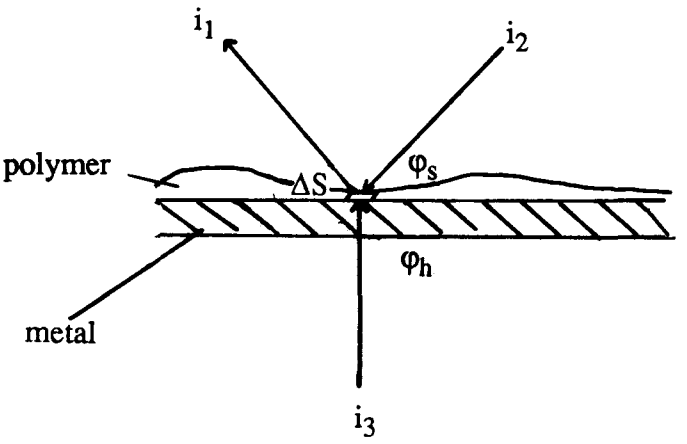

φ_s : the steady state potential,
φ_h : the potential of the sample holder,
i_1 : the electron current emitted from ΔS,
i_2 : the striking current on ΔS from the vacuum space, and
i_3 : the current between ΔS and the spectrometer via the sample holder

Figure 1.3 A schematic diagram of a polymer/metal interface.

where $i_2(0)$ is the striking current at $\varphi_s=0$. At equilibrium $i_1 = i_2 + i_3$, and together with eqs (1.1) and (1.2), we get

$$\varphi_s = [i_1 - i_2(0)] / (c+c') + \varphi_h\, c/(c + c') \qquad (1.3)$$

When the sample holder is grounded ($\varphi_h=0$), the charge build-up is completely determined by the first term of eq (1.3). If different areas of the sample have different photoionization cross sections and electrical characteristics, they will have different i_1, $i_2(0)$, c, c', and hence will have different steady-state potentials, φ_s. That means the sample will develop a non-even surface charging (differential charging).

In contrast, if the sample holder is biased with a sufficiently negative potential, $i_2=0$, and those areas of the interface in good electrical contact with the sample holder will satisfy $\varphi_s=\varphi_h$ since c is large. Those areas that are not located at the interface, or not in good electrical contact with the metal, will create their own φ_s ($=f\varphi_h$). In practice, by shifting the whole spectrum measured for a negatively biased sample back by $-\varphi_h$ eV, those peaks whose positions remain unchanged compared to the non-biased sample must come from regions of the sample in good electrical contact with the metal (i.e. from the interface).

The hypothesis in our work is based upon the above idea. First of all, we assume that silanes and AlO_x may form Al-O-Si bonding. Then two kinds of AlO_x can exist in the interface: the silane bonded and the original. Basically, AlO_x can be treated as conducting material. That implies it will shift by exactly $-\varphi_h$ as an external bias potential is applied. However, when AlO_x forms a bond with the silane, the Al atom in the

Al-O-Si may have a different electrical property than the non-bonded one, with the result that the factor f may change from unity.

D. Aims of Study

The work in this thesis originated from a contract with the Defence Research Establishment Pacific (DREP) to study different corrosion protection treatments on Al alloys and stainless steels. Our present investigation focuses on the adhesion of three organosilanes on 7075-T6 clad Al alloy. This alloy is extensively used for aircraft manufacture. Based upon the work of Matienzo et al [1.33], γ-GPS, γ-APS and γ-MGPS were chosen as model silanes because of their representative behaviors. Although earlier XPS studies of silane/Al interfaces have attempted to study the adhesion bonding, no obvious chemical shift has been assigned to the Al-O-Si bonding. In our work, we assess, for the first time, whether the combination of ADXPS and the bias potential technique [1.38] can give more information on the chemical bonding in silane/Al interfaces.

Two surface treatments were employed in our study. One is organic solvent degreasing and the other is acid etching. Through the ADXPS measurement, the morphology of the differently treated aluminum surfaces can be characterized. From their adhesions with γ-GPS, one can understand how the surface nature determines the bondability of silanes to aluminum.

The organofunctional groups of the silanes actually provide good understanding of their film structures. The amino group ($-NH_2$) in γ-APS is a suitable tag to trace the

molecular film structure. The chemical structure of γ-APS depends on the acidity of the solutions. In aqueous solutions, γ-APS should be in three structural forms: free amino, H-bonded, and protonated -NH_2 groups. With angular dependent measurement, their orientations can be monitored and hence information on the molecular structure of γ-APS films deduced.

Overall, the objective of our work is three-fold. Firstly, coupling of ADXPS with the bias potential technique aims to get direct evidence of the Al-O-Si chemical bonding between silanes and aluminum. Secondly, from the study of degreased Al and acid etched Al, we try to elucidate how physical morphology affects the adhesion. Finally, by monitoring the amino groups, an attempt is made to deduce the film structures of γ-APS at pH=3.0 and pH=10.4.

Chapter 2. X-ray Photoelectron Spectroscopy

A. Historical Development

The history of XPS can be traced back to the work of Hertz [2.1] who produced photoelectrons by illuminating an electrode with ultraviolet light (i.e. photoelectric effect). In 1905, Einstein [2.2] showed that the kinetic energy of a photoelectron is equal to the photon energy minus the electron binding energy and the work function of the solid.

The early XPS experiments were carried out by Robinson and Rawlinson [2.3] before the first World War. They used characteristic Ag and Mo Kα X-ray emission lines to excite photoelectrons. At that time, magnetic analyzers and photographic detectors were used. The resulting spectra consisted of broad bands characterized by high energy edges, which identified the energy levels of the investigated atom. However, there was a large uncertainty in edge positions because of the poor resolution of the energy analyzer. Therefore, XPS remained relatively dormant until the mid 1950's.

In the 1950's, Kai Siegbahn and his co-workers in Uppsala, Sweden, developed a high resolution iron-free double-focussing magnetic analyzer for nuclear spectroscopy of radioactive decay. Later, they realized that the experience from nuclear spectroscopy could be applied to the photoelectric effect [2.4]. The first photoelectron spectrum from cleaved sodium chloride was obtained in 1954. Afterwards, they also found that the core-level binding energies of an element in a molecule was affected by the varying chemical environment. This effect produced a measurable binding energy shift for the photoemission peak. Thus, they coined the acronym ESCA (electron spectroscopy for chemical analysis).

Commercial instruments for XPS appeared around 1969, although initial work was not performed under ultrahigh vacuum (UHV) conditions. Initially, it was thought that XPS characterized the outermost 100 Å of a surface, but the work of Brundle and Roberts in UHV [2.5] in 1972 established XPS as a true surface technique. Presently, XPS spectrometers operate under a pressure of around 10^{-10} torr, normally with a dual MgKα and AlKα anode as the X-ray source.

B. Basic Principles

As noted above, XPS originates with the photoelectric effect; good overview references can be found elsewhere [1.37, 2.6-2.8]. In the measurement, the solid sample is mounted on a sample holder (Figure 2.1), and a source directs soft X-rays towards the sample. In the insert of Figure 2.1, a photon with fixed energy ($h\upsilon$) transfers its energy to a core level electron, which is spontaneously emitted as a photoelectron and measured by the analyzer. A spectrum of photoelectron intensity as a function of binding energy is obtained; those photoemission peaks directly reflect the different orbital energies of the sample.

In the case of a conducting material, the sample and the spectrometer can be in electrical contact, and their resulting energy levels are shown in Figure 2.2 (where several terms are defined). For a metal, the highest occupied energy level defines the Fermi level, while the vacuum level is the energy of an emitted photoelectron at rest in vacuum. According to the conservation of energy:

$$h\upsilon = E_b + E_{k'} + W_s \qquad (2.1)$$

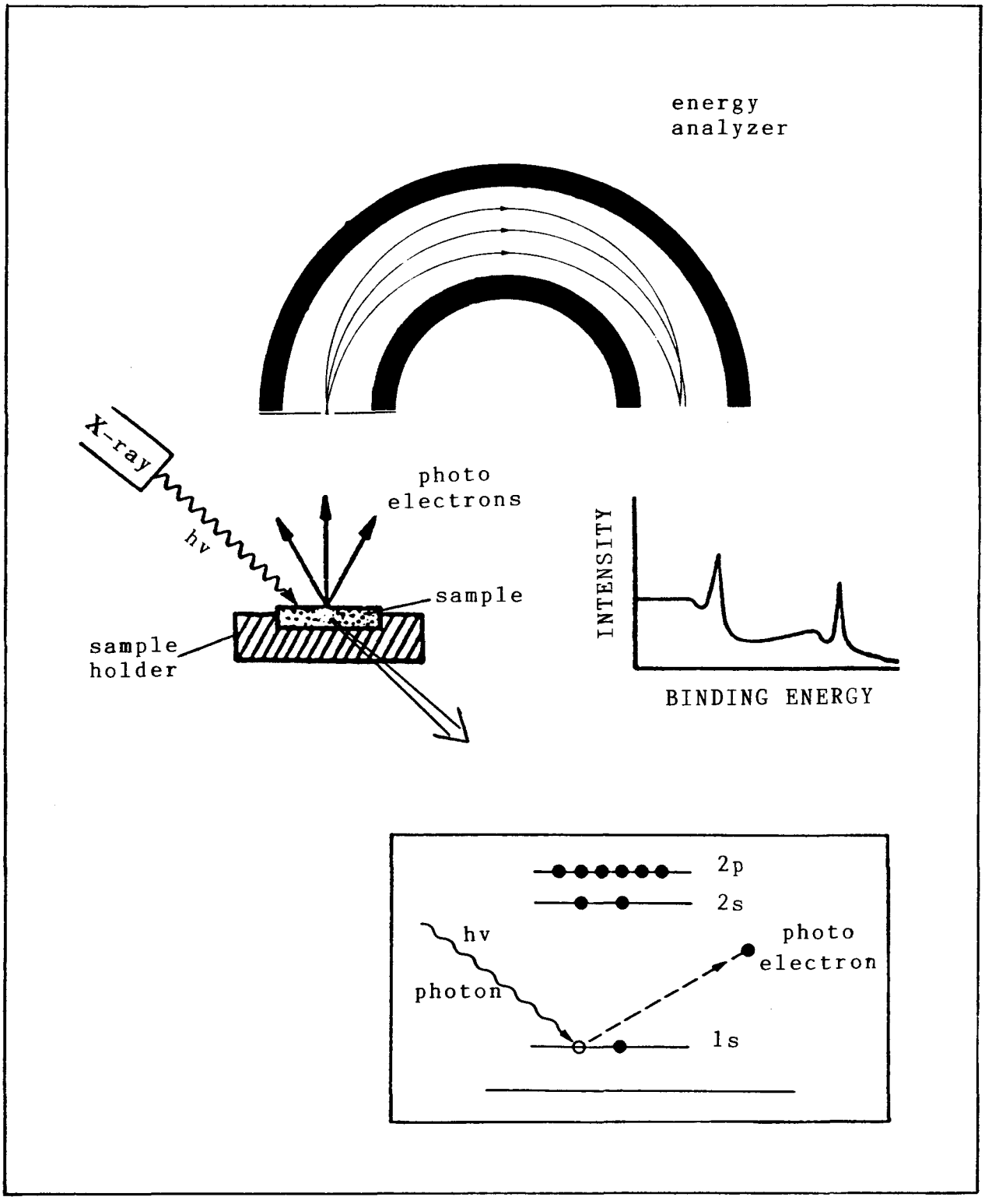

Figure 2.1 Schematic diagram of a X-ray photoelectron spectroscopy experiment. Inserted diagram is the photoelectric process.

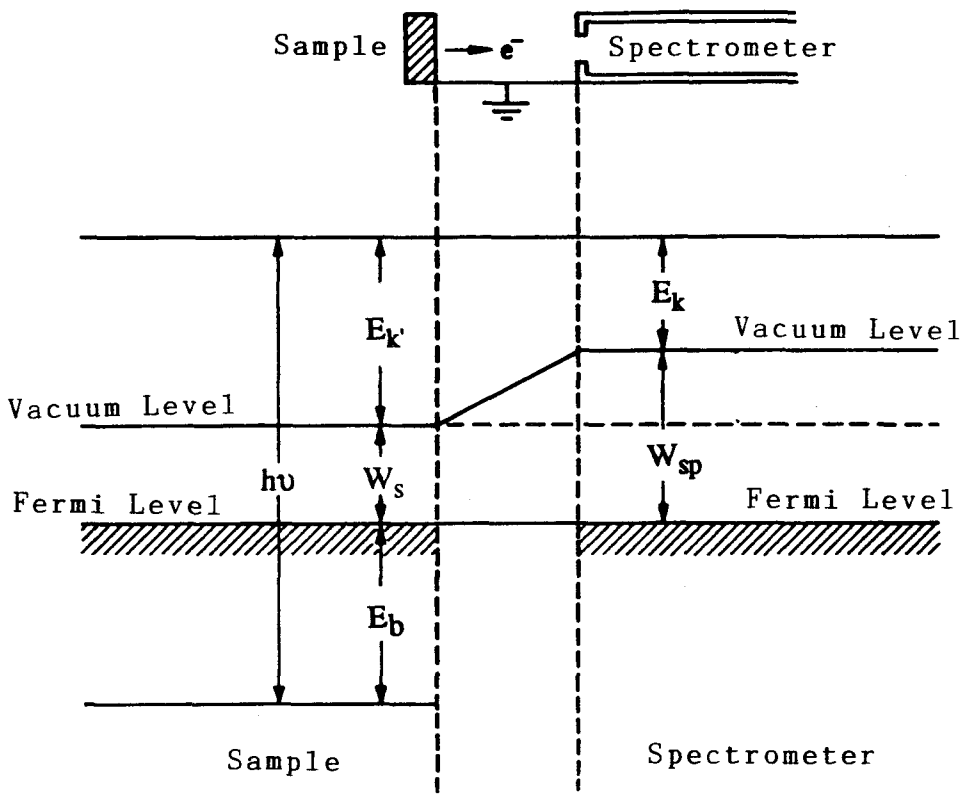

$h\upsilon$ = energy of the photon

W_s = work function of sample (i.e. energy difference between the Fermi level and the vacuum level)

W_{sp} = work function of spectrometer

$E_{k'}$ = kinetic energy of photoelectron with respect to vacuum level of sample

E_k = kinetic energy of photoelectron measured by the spectrometer

E_b = binding energy of electron in solid with respect to the Fermi level

Figure 2.2 Schematic of the relevant energy levels for binding energy measurements.

and so the binding energy for an electron from the sample is:

$$E_b = h\upsilon - E_{k'} - W_s \qquad (2.2)$$

When the specimen is in electrical contact with the spectrometer, their Fermi levels are equal, and so the binding energy can be related to the kinetic energy measured by the spectrometer (E_k) as:

$$E_b = h\upsilon - E_k - W_{sp} \qquad (2.3)$$

W_{sp} is constant for measurements on different samples, although it must be redetermined after each time the spectrometer has been exposed to atmospheric pressure for maintenance or any other purpose.

For different commercial instruments, a variety of source handling techniques are used. So there are different work functions for each spectrometer. Without an defined spectral energy scale, spectra of a sample gathered on different instruments will have different interpretations. That implies a common reference is needed. Most frequently, the $4f_{7/2}$ photopeak from gold at 83.8 eV is used as calibration reference. It is chosen because of its high intensity and accurately known position; also being an inert metal, its binding energy should not be influenced by chemical shifts, nor be shifted by charging effects.

For non-conducting materials the problem is more complicated because of a Fermi level decoupling between themselves and the spectrometer. Now the gold $4f_{7/2}$ peak is no longer a useful reference point. However real samples always contain some

hydrocarbon contamination, and a convenient and usual practice is to take the C_{1s} peak associated with this adsorbed carbon as an internal reference, and to fix it at 285.0 eV.

C. XPS as a Surface Analytical Technique

C-1. Sampling Depth

XPS emphasizes those photoelectrons which do not lose any energy from the point of ionization to vacuum (Figure 2.3). Those electrons that lose energy by scattering inelastically in the solid, contribute to the background or tails of the main signal peaks. The inelastic mean free path (IMFP, λ) is defined as the mean distance travelled by an electron in the solid without losing energy; it provides information on the sampling depth of the XPS technique. Global statements are not readily made, however, because λ is energy dependent (see below). For normal emission, λ relates the intensity (I) obtained from a layer of material (thickness t) and the photoelectron intensity from an infinitely thick layer (I^{∞}), by the equation of (Chapter 2, Section C-5)

$$I = I^{\infty}(1 - e^{-t/\lambda}) \qquad (2.4)$$

By putting $t=\lambda$, $t=2\lambda$, and $t=3\lambda$, it is found that 63% of the total signal intensity is due to electrons originating from a layer thickness of λ, 87% from 2λ and 95% from 3λ. Conventionally, the sampling depth of XPS is taken to equal around 3λ.

λ is a function of electron energy. There are experimental and theoretical approaches for obtaining this parameter [2.9]. Figure 2.4 shows a compilation for

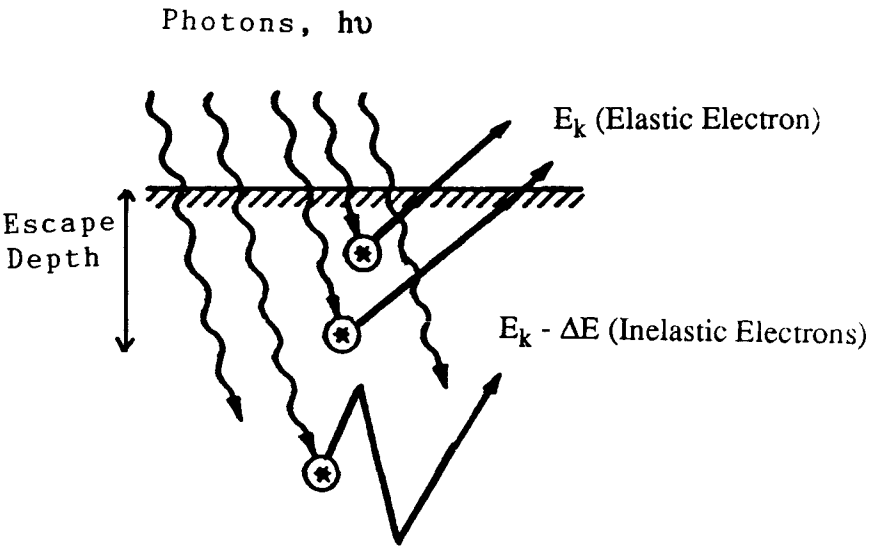

Figure 2.3 Schematic of energetic photons incident on a surface and creating photoelectrons. Only those electrons created near the surface can reach the energy analyzer with no loss of energy.

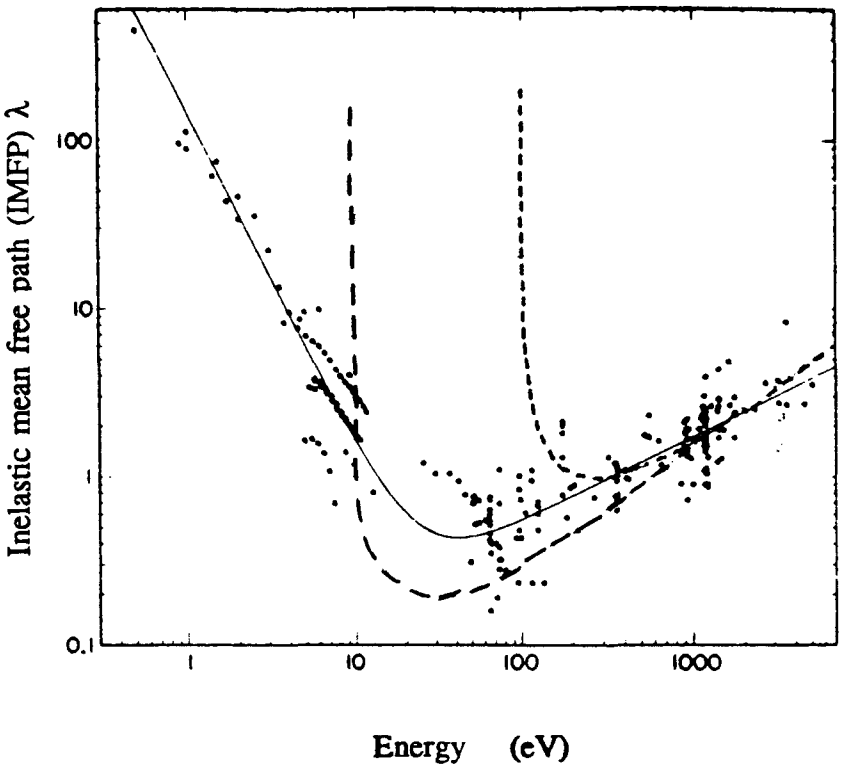

Figure 2.4 Compilation for elements of IMFP measurements in nanometers as a function of energy above the Fermi level. The dashed curves represent theoretical calculations.

elements of IMFP measurements in nanometers [2.9]. The dots are experimental data and the solid curve represents an empirical fit over the complete energy range; the dashed curves are from different theoretical calculations. The measured kinetic energies in XPS generally range from about 100 to 1000 eV. This implies that its sampling depth is typically in the range of 20-80 Å, and hence establishes the reason why XPS is classified as a surface spectroscopy.

C-2. Photoelectron Energy Spectrum

Figure 2.5 represents a wide scan spectrum of gold [2.10] with a MgKα excitation source. The displayed characteristic peaks represent the binding energies of the elastic photoelectrons and directly reflect the core electron structure of the material. The higher energy tails identify inelastically scattered photoelectrons. Since these electrons have lower kinetic energies, they appear as high binding energy tails or background in the spectrum.

The MgKα radiation is only energetic enough to eject the gold core electrons from the 4s shell and above; thus one especially sees ionization from the 4s, 4p, 4d, 4f, and 5d orbitals. Obviously, the different peaks have different intensities and line widths. The non-s levels give doublet structure because of their spin-orbit interactions. The spin orbit peaks are accordingly designated by the subscripts 1/2, 3/2 for p orbitals, 3/2, 5/2 for d orbitals, and 5/2, 7/2 for f orbitals (the peak intensity ratios $(2j_-+1):(2j_+1)$ are 1:2, 2:3 and 3:4, respectively).

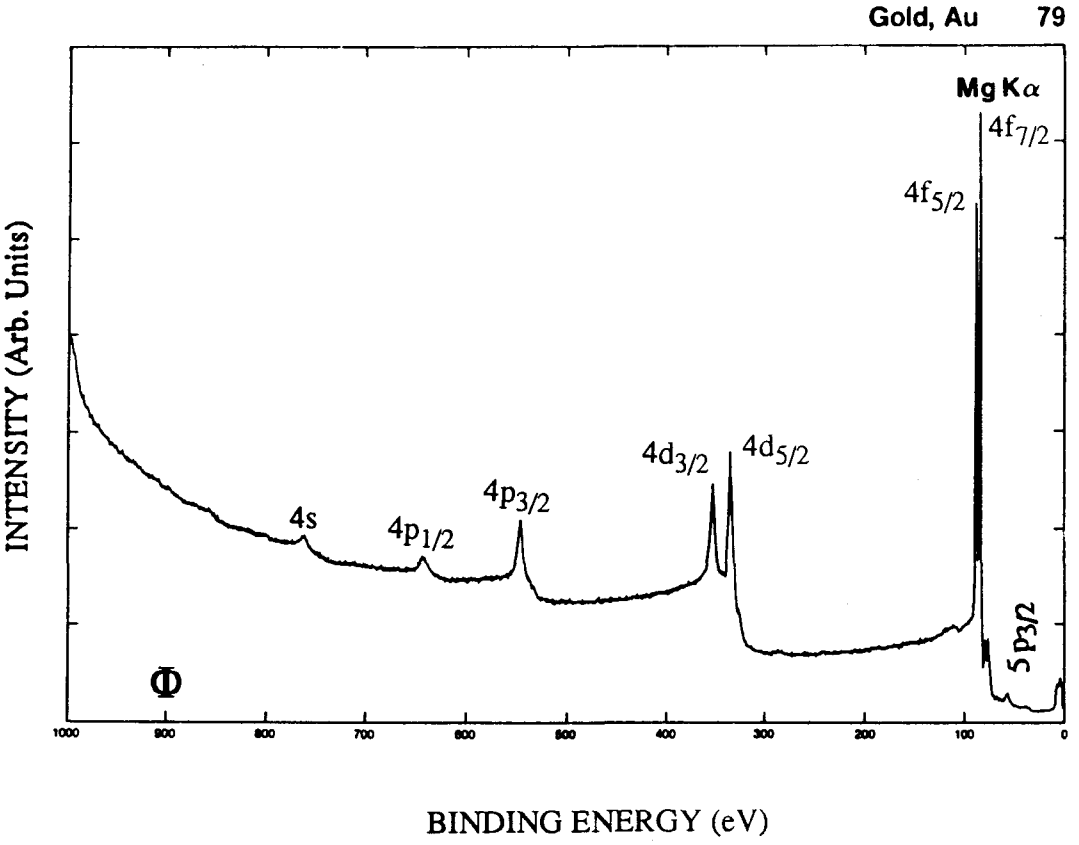

Figure 2.5 A low resolution (wide scan) spectrum for gold with MgKα as the excitation source.

Figure 2.6 shows a narrow scan spectrum for the gold 4f level [2.10]. Key features are the spin-orbit doublet, the background intensity, the peak area and position, and the peak width, which is defined as the full width at half maximum (FWHM, ΔE). The FWHM of a measured photoemission peak depends on the broadening from the X-ray source, the electron energy analyzer, and the natural width of the core level according to:

$$\Delta E_{total} = (\Delta E^2_{source} + \Delta E^2_{analyzer} + \Delta E^2_{line})^{1/2} \qquad (2.5)$$

assuming all lines shapes have the Gaussian form [2.11]. For a given instrument the peak width contribution from source (Chapter 2, Section D-2) and analyzer (Chapter 2, Section D-3) are identical for all photoemission peaks. Therefore, ΔE_{total} directly reflects the uncertainty in the lifetime of the ion state remaining after photoemission.

C-3. Binding Energies and Chemical Shifts

XPS is a straightforward and useful technique for elemental identification in surface regions. Figure 2.7a shows a wide scan spectrum of a 7505-T6 Al alloy panel. The binding energies of the displayed photoemission peaks indicate the presence of aluminum, oxygen and carbon. Detailed listings of major and minor photoemission peak positions can be found elsewhere [2.10].

Figure 2.7b depicts the narrow scan Al_{2p} peak structure for the same aluminum panel. The 2p level of Al has a binding energy of 73.0 eV for metallic Al and of 76.2 eV for Al oxide. Their binding energy difference is around 2.8 eV. Actually, the binding

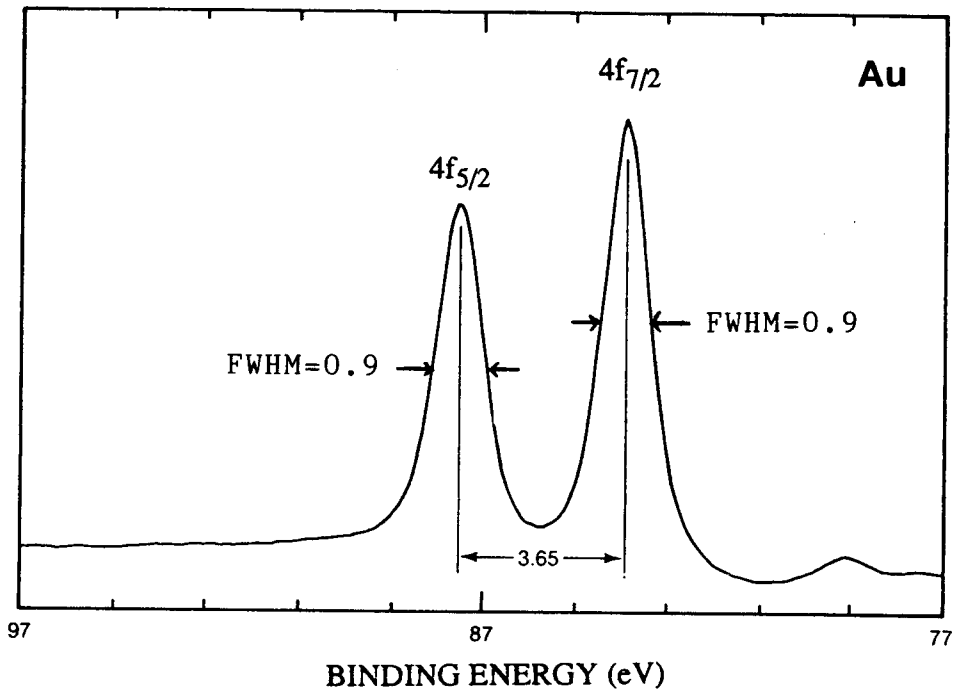

Figure 2.6 A high resolution (narrow scan) spectrum for gold 4f photo-emission peak commonly used for energy calibration of an XPS instrument. The main features of the peak include energy position, peak height, full width at half maximum (both FWHM=0.9 eV), and general peak shape.

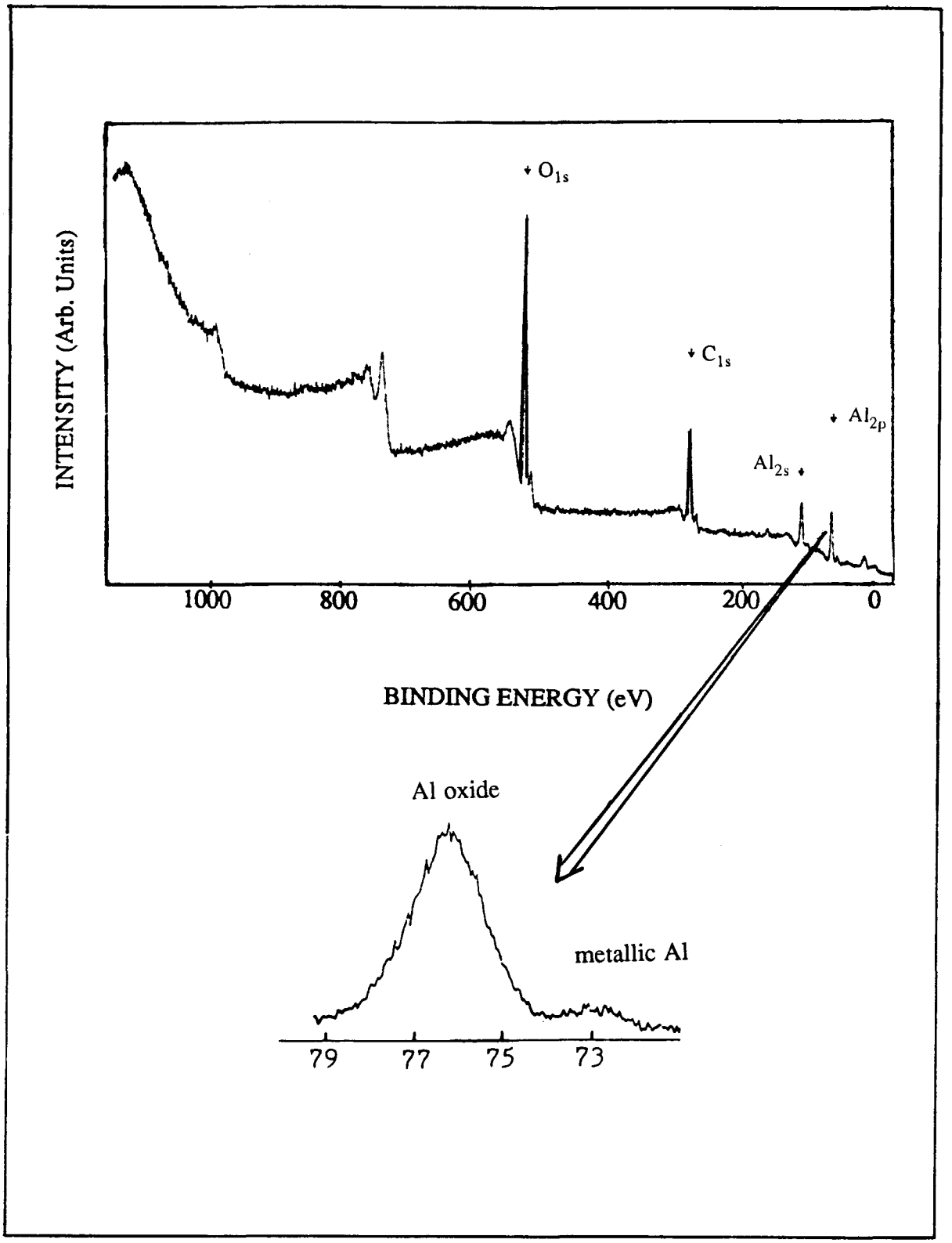

Figure 2.7 XPS spectra for a 7075-T6 Al alloy (a) wide scan and (b) narrow scan for the Al_{2p} photoemission peak.

energy for a photoelectron is governed by the chemical environment experienced by that electron. Let us consider the situation of core electron in an element. The energy of this electron is determined by its Coulomb interaction with the other electrons and the attractive potential of the nuclei. Any change in the chemical environment of the element will redistribute its valence electrons, and a different potential will be created and seen by the considered electron. Compared with the metal, Al photoelectrons from the oxide experience less electron repulsion and greater nuclei attraction because of the higher oxidation state; as a result, a binding energy difference (or chemical shift) arises which is easily measurable in XPS.

Chemical shifts are commonly used to identify the chemical environments of an atom. By comparison with the binding energies of reference compounds, one can get the chemical state of a particular atom in a sample. A compilation of the binding energies of different elements and compounds has been presented in XPS handbooks [2.10].

C-4. Quantitative Analysis

Peak intensities (i.e. areas under photoelectron peaks) are of interest for quantitative analysis in XPS. For a homogenous solid element of infinite thickness, the intensity of a photoemission peak can be expressed as:

$$I^{\infty} = nf\sigma\Theta y\lambda AT \qquad (2.6)$$

or

$$n = I^{\infty}/f\sigma\Theta y\lambda AT$$

$$n = I^{\infty}/S \qquad (2.7)$$

where n = number of atoms of that element per unit volume (cm^{-3}), i.e. atomic density,

f = the x-ray flux (photons/cm^2 sec),

σ = the photoionization cross section (cm^2),

Θ = an angular efficiency factor for the instrumental arrangement

y = the efficiency in the photoelectric process

λ = the inelastic mean free path,

A = the sampling area,

T = the detection efficiency for the emitted electron, and

S = elemental sensitivity factor.

The use of elemental sensitivity factors has been proposed and developed by a number of authors [2.12]. Extensive measurements have been made [2.13, 2.14]. These authors developed a relative scale in which elemental intensities were referenced to the F_{1s} intensity and S is assumed to be a constant for a given element and photoemission peak. Tables of sensitivity factors for a given spectrometer are determined by measuring reference peak intensities with the instrument. Relative atomic concentrations of any constituent in a sample surface can be obtained by:

$$C_x = n_x / \Sigma n_i = (I_x/S_x)/ \Sigma (I_i/S_i) \qquad (2.8)$$

Quantitative data in XPS are conventionally given in terms of numbers of atoms, hence elemental concentrations are in atomic percentages rather than weight ratios.

C-5. Angular Dependent Measurements

The basic idea of surface sensitivity enhancement by varying the take-off angle (θ, angle between the plane of the surface and the axis of the energy analyzer) is illustrated in Figure 2.8. At normal take-off angle (θ=90°), the sampling depth is 3λ. At grazing angles of emergence, the sampling depth is reduced to $3\lambda\sin\theta$. That implies with low take-off angle, the surface sensitivity of the measurement increases (a review can be found in reference [2.15]). Figure 2.9 shows the Al_{2p} photoemission peak for a 7075-T6 Al panel with the take-off angle varying from 90° to 45°. Since metallic Al stays deep below and the Al oxide lies above, so the metallic peak is most intense at θ=90° and gradually disappears as θ decreases.

Figure 2.10 depicts several overlayer/substrate geometric models [2.16]. For case a with a thin overlayer ($t<3\lambda_s$), the intensity of the substrate, I_s, can be expressed as

$$I_s = (I_s)^{\infty} \exp(-t/\lambda_s \sin\theta) \qquad (2.9)$$

while the intensity of the overlayer, I_o, is

$$I_o = (I_o)^{\infty} [(1 - \exp(-t/\lambda_o \sin\theta)] \qquad (2.10)$$

λ_o and λ_s are the IMFP of the substrate and the overlayer respectively. $(I_o)^{\infty}$ and $(I_s)^{\infty}$ can be derived from eq (2.6). The intensity ratio, $R(\theta)$ between I_o and I_s is

$$R(\theta) = (I_o/I_s)^{\infty}[1 - \exp(-t/\lambda_o \sin\theta)] \exp(t/\lambda_s \sin\theta) \qquad (2.11)$$

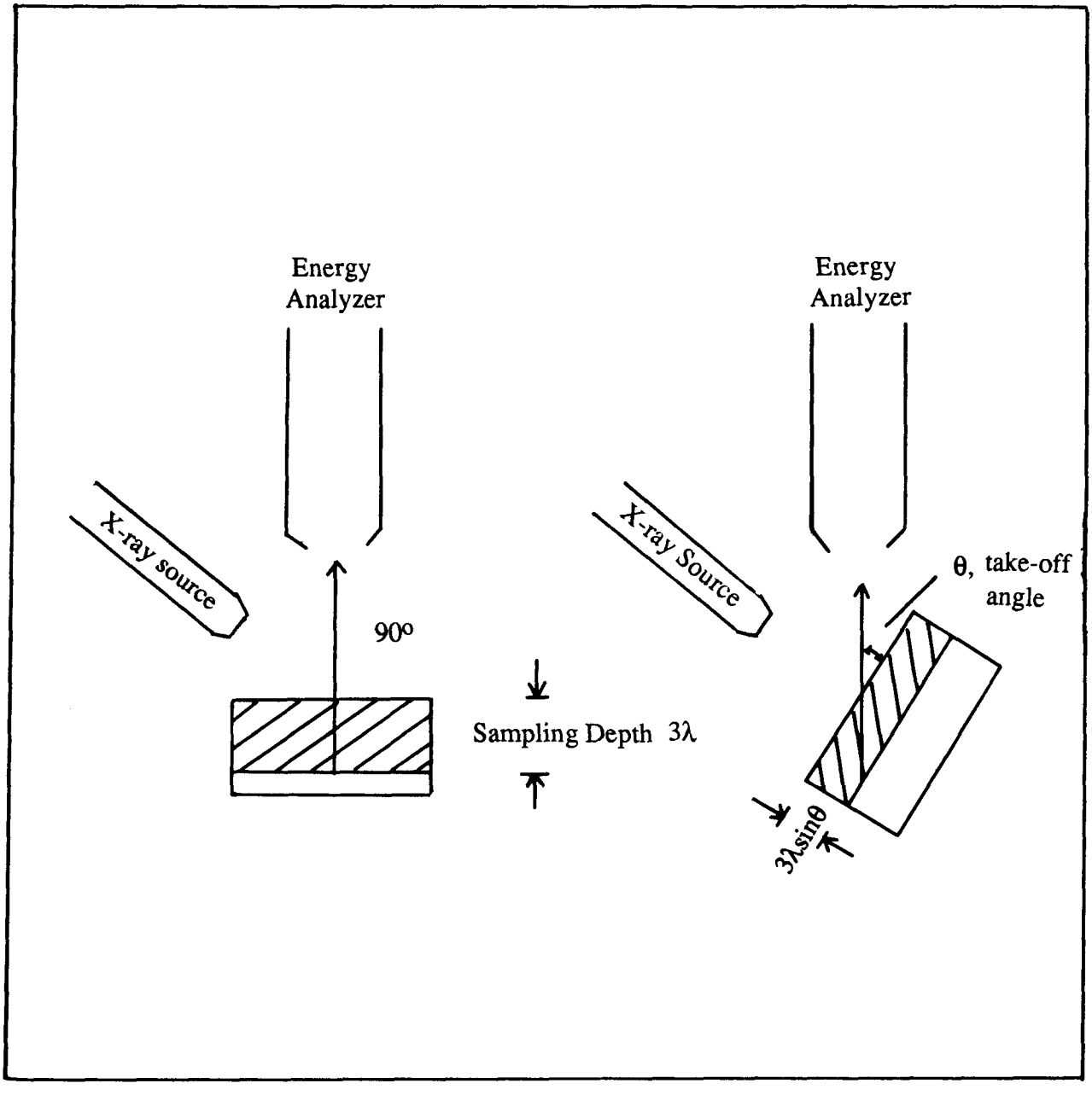

Figure 2.8 Surface sensitivity enhancement by varying the take-off angle. The sampling depth changes from 3λ to $3\lambda\sin\theta$ as take-off angle decreases from 90^{o} to θ.

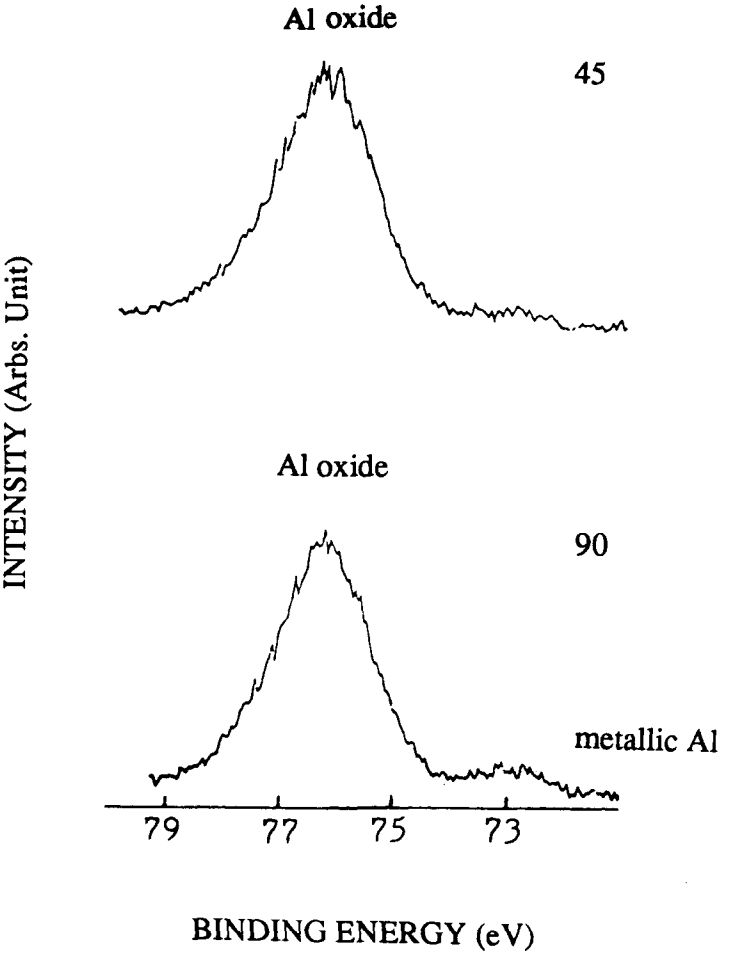

Figure 2.9 Al_{2p} spectra for a 7075-T6 Al alloy for take-off angles $\theta=90^{o}$ and 45^{o}.

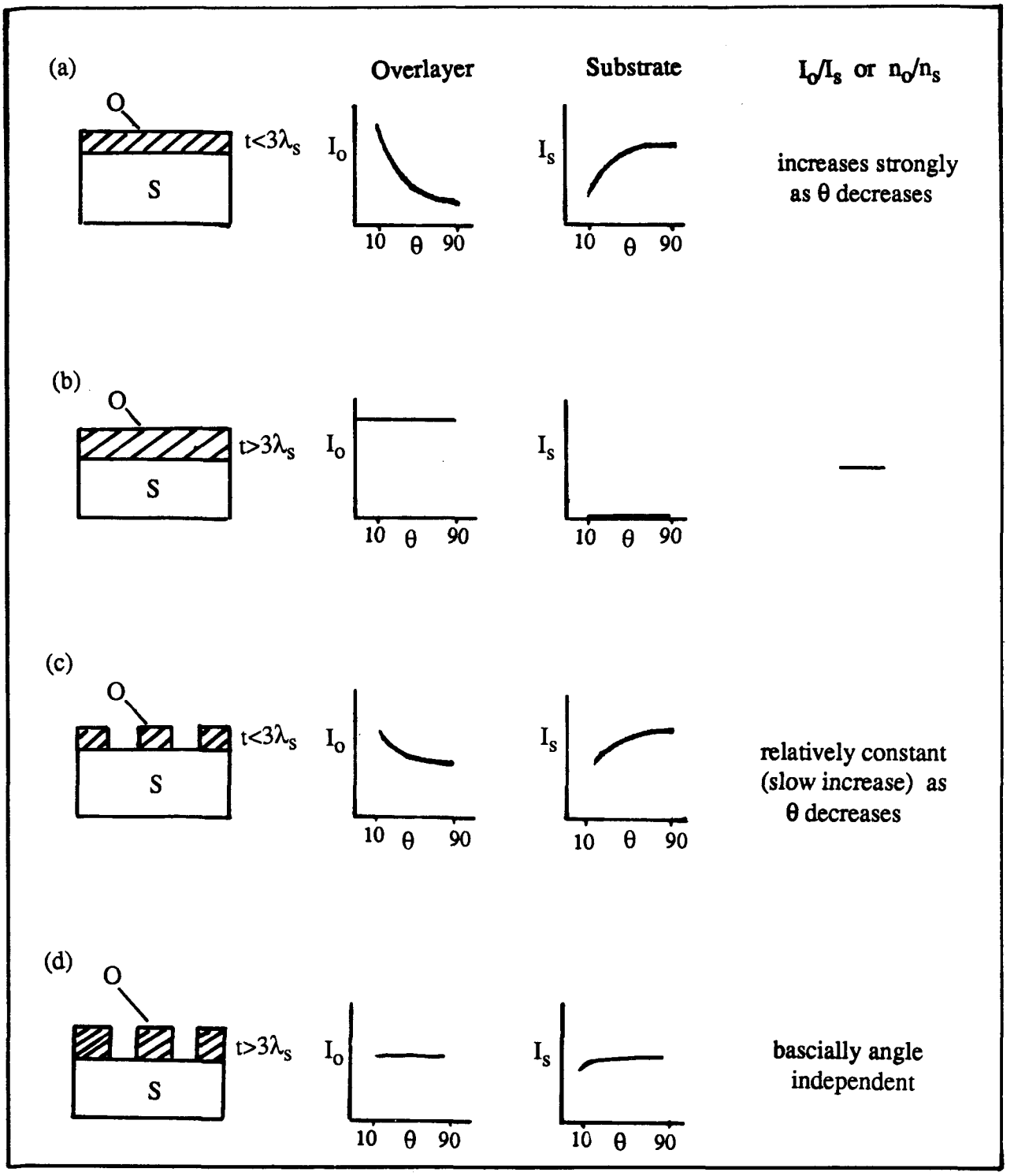

Figure 2.10 Variation of overlayer and substrate photoelectron intensities for four models of a surface [2.16] (a) continuous overlayer with $t<3\lambda_s$, (b) continuous overlayer with $t>3\lambda_s$, (c) patchy overlayer with $t<3\lambda_s$, and (d) patchy overlayer with $t>3\lambda_s$.

and R(θ) increases steadily as θ decreases. If $(I_O)^\infty/(I_S)^\infty$ is a constant, and $\lambda_O = \lambda_S$, eq (2.11) becomes

$$R(\theta) = K \exp [(t/\lambda_S \sin\theta) - 1] \qquad (2.12)$$

$$\ln R(\theta) = (\ln K - 1) + t/\lambda_S \sin\theta$$

Eq (2.12) provides a linearized method for plotting experimental lnR(θ) data against 1/sinθ to determine the overlayer thickness t (from t=slope x λ_S).

In case b, the substrate is covered by an overlayer with thickness greater than $3\lambda_S$. Here the photoelectrons from the substrate can no longer penetrate the overlayer, so I_S is effectively zero.

In case c, with a thin patchy overlayer, I_S depends on the extent of coverage and the precise thickness of the overlayer, while in case d, with a thick patchy overlayer, I_O and I_S depend upon the geometry of the system. At low angles I_S will be shadowed by the overlayer, resulting in a rapid decrease in signal intensity with decreasing θ. Overall, for substrates with patchy overlayers, the intensity ratio of the overlayer and substrate signals is not angle dependent. In practice, the atomic ratios of the overlayer and the substrate (n_O/n_S) can also be used to monitor the surface morphology ($I_O/I_S = C \times n_O/n_S$, C=elemental sensitivity ratio).

Since angle dependent XPS measurements (ADXPS) can give atomic concentrations at different depths, it naturally creates a non-destructive depth profile for the sample. Practically, the usefulness of ADXPS is most prominent in cases a and b. The atomic ratios can be used to interpret the relative orientation of one species to another or the

composition gradient of the overlayer. On the other hand, the atomic ratios in cases c and d cannot provide much information on this aspect (their ratios are always constant or random).

D. Instrumentation

A typical XPS instrument basically consists of an X-ray source, a sample mounting assembly, an analyzer, a detector, data processing devices and an output display. In our laboratory, a Leybold MAX 200 spectrometer is operated [2.17]. Figure 2.11a schematically shows the side view, and Figure 2.11b gives its main components. In addition to the main parts stated above, the MAX 200 system has a flood gun for discharging the surface, an ion gun for sputtering and ion scattering spectroscopy, an X-ray monochromator (for better X-ray resolution), and some additional surface science equipment. Considerations for the UHV system [2.17, 2.18], the X-ray source [2.18], and the energy analyzer [2.18] are discussed first, and later there are discussions of the sample handling and data analysis [2.17].

D-1. UHV System

The chambers of a modern spectrometer are constructed of stainless steel. In order to reach UHV condition in a reasonable time, it is necessary to pump away gases adsorbed on the chamber walls at a fast rate. This can be accomplished by baking the chamber to about 150 °C for a few hours while pumping. During the cooling down to room temperature, the outgassing rate from the internal surfaces drops and the pumps are

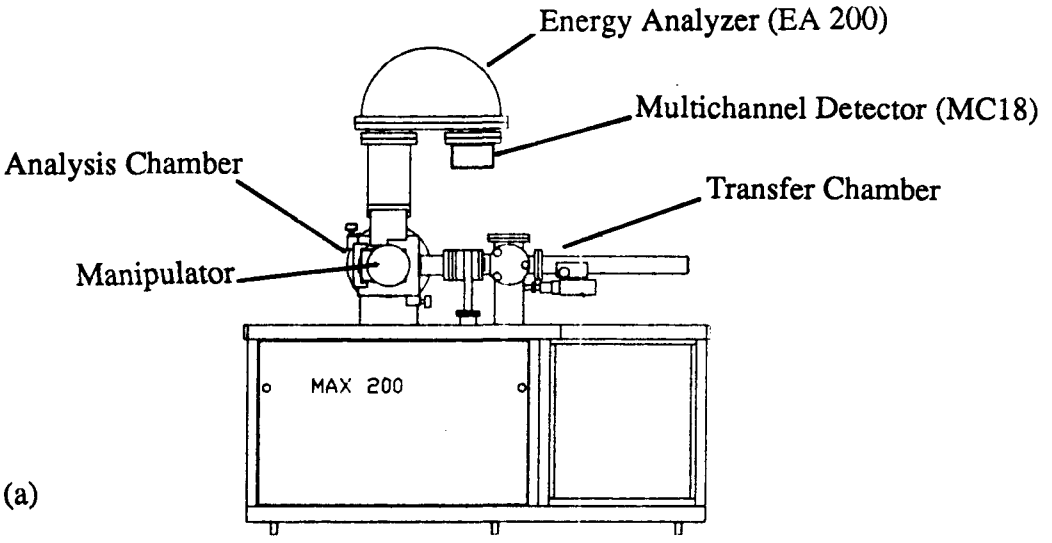

(a)

Energy Analyzer (EA 200)

X-ray monochromator (RMC10)

X-Ray source (XR 200)

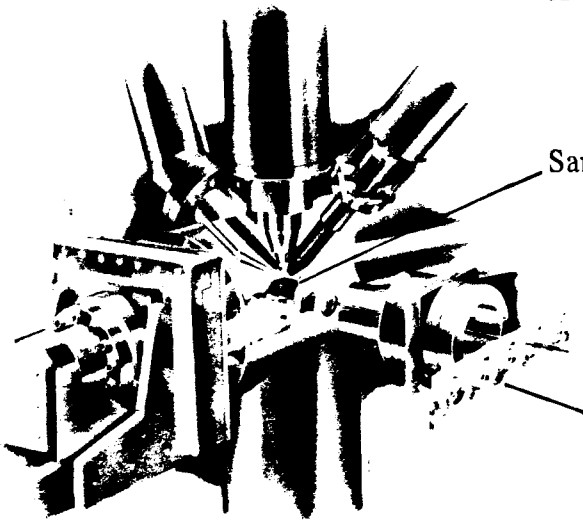

(b)

Figure 2.11 Schematic diagrams of (a) the side view and (b) the individual parts of MAX 200 system.

then capable of producing and maintaining the UHV. Diffusion, sputter ion, turbomolecular, and titanium sublimation pumps may be used in various combinations in different commercial spectrometers.

Figure 2.12 represents the pumping system of the MAX 200 system. Pressures of the transfer chamber and the analysis chamber are reduced from 1 atm to 10^{-3} torr by a rotary pump, then the turbomolecular pumps further reduce the pressures down to the 10^{-8} torr range. A separate differential ion pump is operated for the X-ray source. Typically, the base pressures are $3x10^{-10}$ torr in the analysis chamber and $1.5x10^{-8}$ torr in the transfer chamber.

D-2. X-ray Sources

When choosing material as the anode of an X-ray source, two aspects must be taken into consideration. On one hand, the energy resolution should be good. Mostly, it is necessary to use a material with line width (i.e. FWHM, ΔE) less than 1.0 eV. On the other hand, the emitted X-ray of that material must be energetic enough to excite the core electrons of most elements. Table 2.1 [2.18] lists some characteristic X-ray lines with their corresponding energies and line widths. MgKα and AlKα provide a good compromise of high energy and narrow line width, and these two sources are very commonly used in XPS.

During operation, a filament is heated and the emitted electrons are accelerated (to ~20 kV) and directed on to the anode. This impact induces the emission of X-ray radiation. For purposes of optimizing sensitivity at a given energy resolution, it is

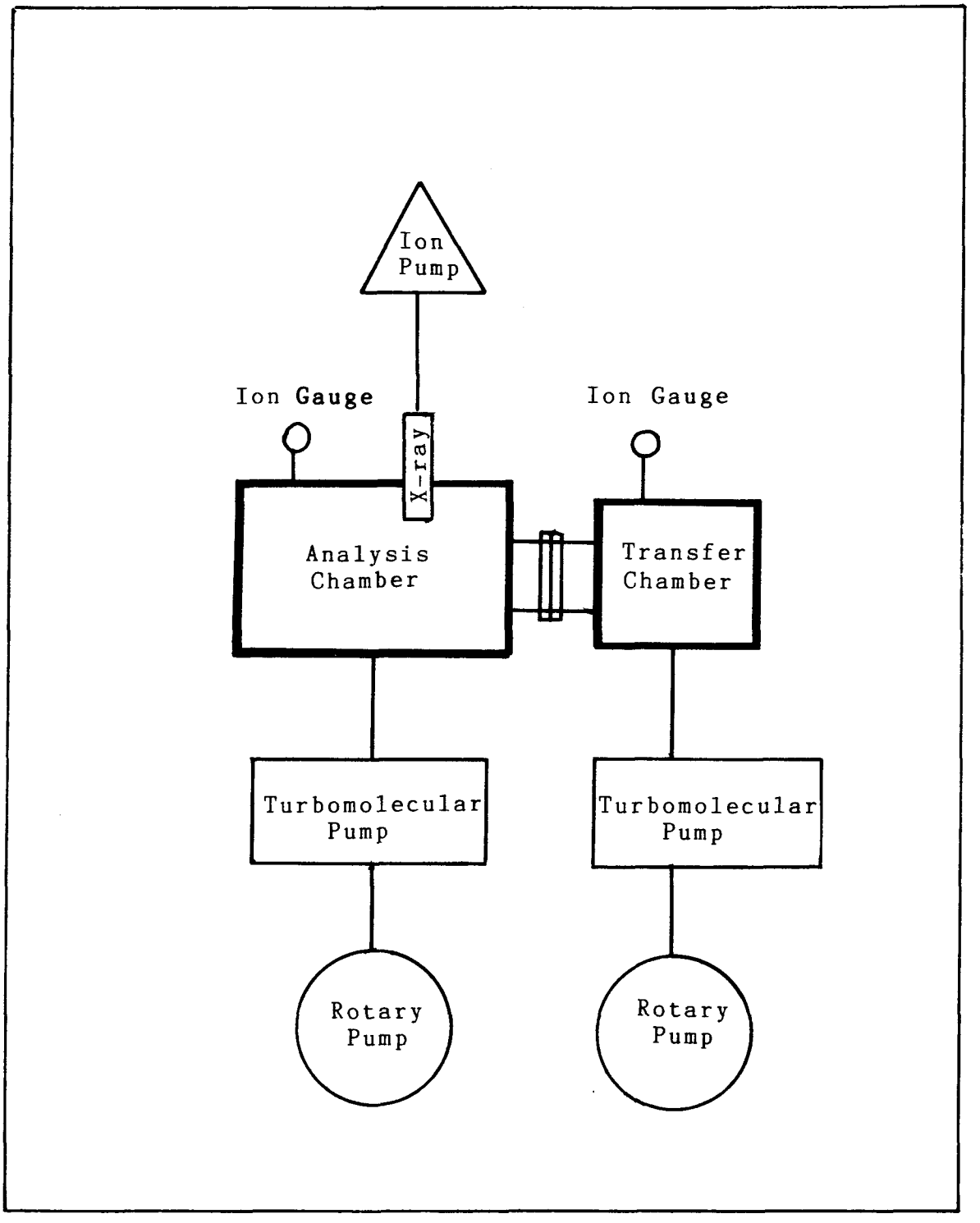

Figure 2.12 Pumping system for the MAX 200 system.

Table 2.1 Energies and widths of some characteristic soft X-ray lines [2.18]

Line	Energy, eV	Width, eV
YMζ	132.3	0.47
ZrMζ	151.4	0.77
MbMζ	171.4	1.21
MoMζ	192.3	1.53
TiLα	395.3	3.0
CrLα	572.8	3.0
NiLα	851.5	2.5
CuLα	929.7	3.8
MgKα	1253.6	0.7
AlKα	1486.6	0.85
SiKα	1739.5	1.0
YLα	1922.6	1.5
ZrLα	2042.4	1.7
TiKα	4510.0	2.0
CrKα	5417.0	2.1
CuKα	8048.0	2.6

necessary to use as high an electron bombarding current as the source can stand since the photon flux is directly proportional to that current. In most source control units the bombarding current can be selected in a continuous range. Inside the anode, deionized water is circulated for heat removal during the high voltage electron bombardment. The X-ray source used in our work has the dual anode design (Figure 2.13); although the MAX 200 system also has an AlKα monochromator. The dual anode source has two filaments for electron bombardment and two anodes surfaces, one of Mg and one of Al. It is possible to switch from one source to the other in a few seconds. It is desirable to have the dual anode facility because these two X-ray sources have different line widths (0.70 eV for MgKα and 0.85 eV for AlKα). Owing to its higher energy, AlKα is more frequently operated because a greater energy range spectrum can be obtained. If better resolution is required, the MgKα or monochromatized AlKα sources are used. Another reason for using two sources in XPS analysis is that peak overlaps can result in an obscuring of photoelectron and Auger peaks. By switching the excitation source, any such overlaps are resolved because the Auger peak energies are independent of the photon energy, while the XPS energies vary directly with the source energy.

To screen out stray electrons from the X-ray source reaching the sample or the analyzer, a thin Al foil (about 2 μm in thickness) window is interposed between the anode and the sample. For that thickness the X-ray flux received by the sample attenuates by about 24% for MgKα and 15% for AlKα. During sputtering, a shutter will flip in front of the Al window to protect the X-ray source from damage caused by the sputtered ion fragments.

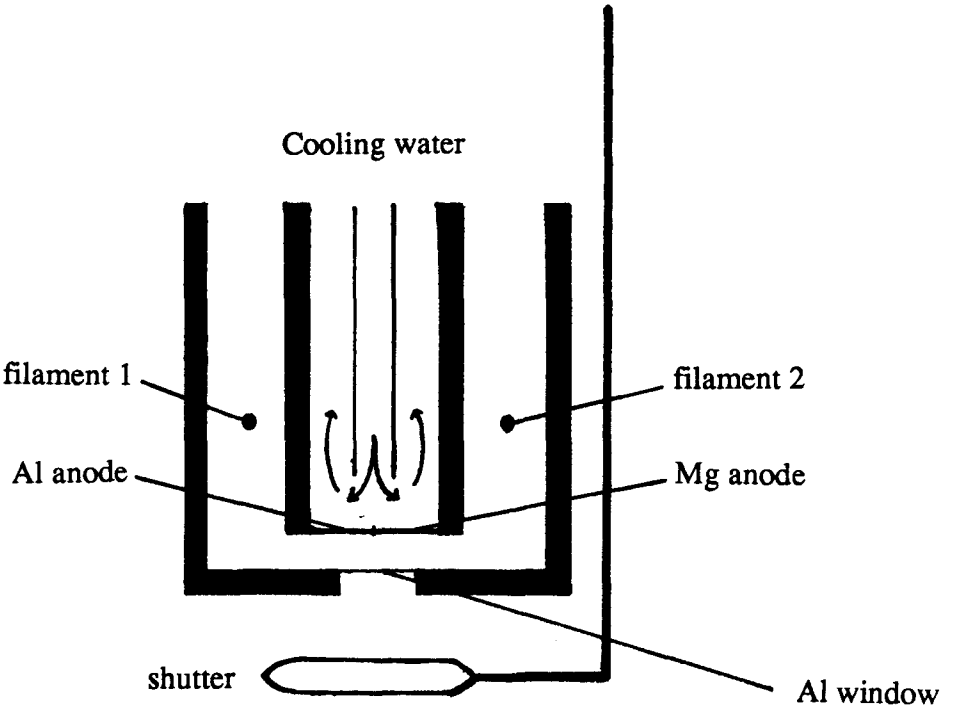

Figure 2.13 A schematic diagram of a Mg/Al dual anode X-ray source (XR 200) in MAX 200 system.

D-3. Energy Analyzer

The concentric hemispherical analyzer (CHA) is the most widely used energy analyzer in XPS, and its schematic structure is illustrated in Figure 2.14a. The CHA consists of two concentric hemispheres (inner radius R_1, outer radius R_2) and a potential is applied across the hemispheres such that the outer one is negative and the inner positive. For an applied potential difference (ΔV) between the hemispheres, the condition for an electron of kinetic energy E_o to pass through the analyzer is given by:

$$e\,\Delta V = E_o\,(R_2/R_1 - R_1/R_2) \qquad (2.13)$$

That means, for a particular voltage setting, only electrons whose kinetic energies are in a narrow band to satisfying eq (3.11) can reach the exit slit. Those with energies greater or lower than E_o will be attracted to the walls of the hemispheres and hence will not be detected.

The resolution (R) of a CHA, which is one contribution of the photoemission peak width (eq (2.5)) can be written as

$$R = \Delta E_{analyzer}/E_o = w/2R_o + \alpha^2/4 \qquad (2.14)$$

where $\Delta E_{analyzer}$ = the photoemission peak broadening contributed by the analyzer

w = the slit width (in radian)

α = entering angle (in radians)

R_o = the median equipotential surface between the hemispheres (i.e. $(R_1+R_2)/2$)

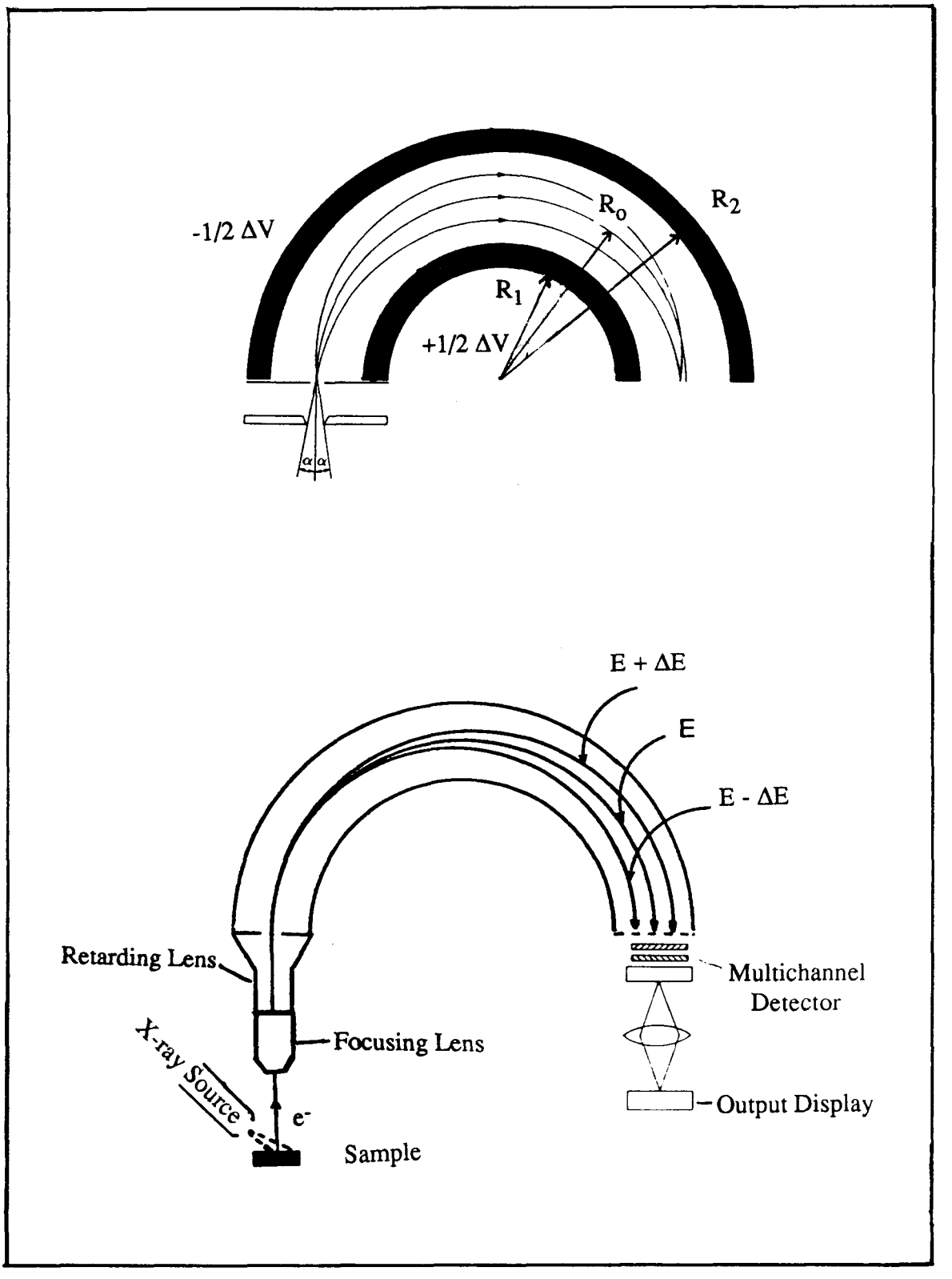

Figure 2.14 (a) A schematic concentric hemispherical energy analyzer (CHA)

(b) A schematic CHA (EA 200) in MAX 200 system.

The resolution of the CHA is fixed by w and α. Although R is constant across the entire measurement of a spectrum, $\Delta E_{analyzer}$ varies for each photoemission peak (the greater the kinetic energy of the detected electron, the greater is $\Delta E_{analyzer}$). For this reason, all photoelectrons to be studied are retarded to a constant pass energy before entering the analyzer; then the resolution associated with the analyzer is identical for each photoemission peak.

During data acquisition, a pass energy is chosen and fixed according to the level of resolution needed. The potential of the analyzer, ΔV, is set according to eq (2.13) for that particular pass energy. The actual scanning of kinetic energy is thus done by ramping voltages in the pre-retardation section; this energy retardation is achieved by a set of lenses coupled with the analyzer. After retarding to the pass energy, electrons pass between the hemispheres and are collected on to a channelplate detector.

In principle, a low pass energy would give better analyzer resolution, but the signal intensity drops off rapidly with retardation. Therefore, the pass energy should be chosen to get the optimal balance between resolution and intensity. Figure 2.14b gives a schematic indication of the MAX 200 energy analyzer (EA 200, 150 mm radius) which is coupled with the retarding lens and the electron focusing lens. In order not to damage the sample surface, the high-intensity X-ray source is not focused in the MAX 200. However, when micro area analysis is performed, the focusing lens is used to collect the photoelectrons from restricted regions of the surface.

D-4. Sample Handling

In XPS analysis, samples are often studied in the "as received" condition. In the MAX 200, samples can be mounted on standard sample holders and locked on a sample magazine (shown in Figure 2.11b) which can hold up to seven sample holders. The sample magazine then is introduced to the transfer chamber prior to the initial pumpdown. Once the transfer chamber pressure is reduced to 10^{-8} torr, one sample holder will be transferred to the analysis chamber and locked to the manipulator. With this manipulator, the sample can be given five degrees of movement (three for linear and two for rotational). This enables proper positional settings and the ability to perform angle dependent measurements in the analysis.

D-5. Data Analysis

The MAX 200 XPS spectrometer collects data digitally and is interfaced to a HP 1000 based microprocessor using Data System DS 100 software. The selection of instrumental parameters, and operations of data acquisition and data processing are controlled by the computer.

Raw spectra are background subtracted before performing any data analysis, then an energy calibration is needed, following the approaches noted in chapter 2, section B. The gold $4f_{7/2}$ peak at 83.8 eV is commonly used for calibrating metallic photoemission peaks. Practically, a gold spectrum is scanned with a normally used pass energy for high resolution scans. Then the gold $4f_{7/2}$ peak is tuned exactly at 83.8 eV; all spectra afterward will be calibrated against this standard reference before displaying. In the case

of non-conducting materials, C_{1s} at 285.0 eV is used as internal reference. If, the C_{1s} peak appears at 287.0 eV, the entire spectrum is simply shifted back by 2 eV. The calibration must be performed individually for each spectrum from insulating samples. After the energy calibration, the binding energies of each photoemission peak in a wide scanned spectrum can be used for elemental identification. For quantitative measurement, the area under each peak is integrated, and with the set of sensitivity factors for the instrument, elemental percentages of samples determined.

High resolution, narrow scanned photoemission peaks can provide a good deal of chemical information. Often these peaks are not symmetrical, and they consist of several components, each corresponding to a different chemical state. These components can be separated and resolved by mathematical curve analysis carried out on the microcomputer system. This analysis identifies superimposed peaks or doublets in a measured peak, and the results of the fit can be rapidly displayed together with quantitative information. The software in the MAX 200 system fits to individual mixed Gaussian/Lorentzian functions:

$$f(E) = \text{peak height} / [1 + M(E-E_o)^2/\beta^2] \exp \{(1-M) [\ln 2(E-E_o)^2]/\beta^2\} \qquad (2.15)$$

where $f(E)$ = the intensity of the fit function

E = the corresponding kinetic energy

E_o = the peak centre

β = a parameter from which the actual FWHM is calculated

M = the mixing ratio (1 for a pure Lorentzian peak;
0 for a pure Gaussian peak)

All parameters including the peak position, intensity and the FWHM are initially estimated and then optimized. The goodness of fit is evaluated by the chi-square (χ^2) function:

$$\chi = \{1/N_{free} \times \Sigma_{i=1} (Y_{mea} - Y_{fit})^2/Y_{mea}\}^{1/2} \qquad (2.16)$$

and Y_{mea} = the measured count rate

Y_{fit} = the intensity value of the fit function

N_{free} = N - N_{fit} (N is number of points in the fit region and N_{fit} is the number of fit parameters)

If the curve analysis is repeated with a different set of parameters, the new chi value will indicate whether the operation has improved the previous fit or not. The smaller χ^2 value, the better is the fit.

The optimal application of curve fitting methods requires some knowledge about the chemistry of the system, to be sure that a proposed fitting is reasonable. Let us consider a narrow-scan C_{1s} peak for a γ-GPS polymeric film as shown in Figure 3.4a. The peak shape tells us that it contains more than one component. From the chemical formula of the silane (see Table 1.1), it is clear that two kinds of carbon exist. One is the hydrocarbon (C-C), and the other is the glycixdoxy and epoxy (C-O). In the fitting process, two components are assigned for the C_{1s} peak. With their estimated peak positions, peak heights and FWHM, the curve fitting analysis gives two components: one at 285.0 eV for (C-C) carbon and the other at 286.5 eV for (C-O) carbon.

Chapter 3. Studies on Silane/Aluminum Interfaces

A. Sample Preparations

The samples studied in this work are designated below by the labels A to I (Table 3.1). The 7075-T6 aluminum sheets were obtained from the Defence Research Establishment Pacific (DREP). All samples used panels 1 cm x 1cm in area, which were degreased in acetone and rinsed in distilled water before further treating. Those panels which received an etching treatment were subjected to a chromic acid/sulfuric acid solution (an aqueous solution of 60 g/l sodium dichromate dihydrate and 17 vol% sulfuric acid [3.1]) for 15 min at 65 °C, then rinsed in distilled, deionized water and air dried.

1 vol% solutions of γ-GPS [$(CH_2CHCH_2O(CH_2)_3Si(OCH_3)_3$], γ-APS [$NH_2(CH_2)_3Si(OCH_3)_3$] and γ-MGPS [$HS(CH_2)_3Si(OCH_3)_3$] were prepared by dissolving their monomers in the solvent formed by 50 vol% distilled water and 50 vol% methanol respectively. The acidic γ-APS solution was prepared by adding HCl to natural 1% γ-APS solution (pH=10.4) until pH=3.0.

B. XPS Measurements

All XPS spectra were measured in the MAX 200 spectrometer at an operating pressure of about 4.5 x 10^{-9} torr. The unmonochromatic MgKα excitation source was operated at 15 kV and 20 mA. Emitted photoelectrons were obtained from a 2 x 4 mm^2 area. Wide scan spectra, mainly for qualitative elemental determination, were obtained with the pass energy set at 192 eV; narrow scan spectra for quantitative and chemical state analysis had the pass energy set at 48 eV. Relative elemental percentages were

Table 3.1 Sample Preparations

Method of Modification	Chemical type	Code in Text
Degreased Al panel.	Degreased	A
Degreased Al panel followed by acidic chemical etch.	Degreased and acid etched	B
Sample B immersed in 1% γ-GPS for 2 hr and air dried.	Polymerized γ-GPS film	C
Sample C rinsed in deionized water after removing from the spectrometer	Polymerized γ-GPS film	D
Sample A immersed in 1% γ-GPS for 2hr, air dried and rinsed with deionized water.	γ-GPS/Al interface (I)	E
Sample B immersed in 1% γ-GPS for 2 hr, air dried and rinsed with deionized water.	γ-GPS/Al interface (II)	F
Sample B immersed in 1% γ-APS (pH=3.0) for 15 min and air dried.	γ-APS/Al interface (I) (pH=3.0)	G
Sample B immersed in 1% γ-APS (pH=10.4) for 15 min and air dried.	γ-APS/Al interface (II) (pH=10.4)	H
Sample B immersed in 1% γ-MGPS for 5 min and air dried.	γ-MGPS/Al interface	I

obtained by integrating corresponding peak areas after making background subtraction and a sensitivity factor correction. The gold $4f_{7/2}$ photoemission peak at 83.8 eV was the reference to calibrate other core level peaks. Angle dependent spectra were measured by varying the angle between the plane of the sample surface and the axis of the analyzer. A -93 V potential was applied to samples E to I during the biasing experiment. Afterwards, all the biased spectra were mathematically shifted back by 93 eV for comparing with their own non-biased spectra.

C. Results and Discussion

C-1. Aluminum Control Surfaces

Figure 3.1 shows the C_{1s} and Al_{2p} peaks for sample A (the degreased Al panel) and sample B (the acid etched Al panel) at θ=90°. The carbon signals possibly arise from airborne contamination or some residual acetone used in the degreasing procedure. Three components are assigned in the curve analysis. They are C-C component at 285.0 eV, C-O component at 286.7 eV, and C=O component at 288.9 eV. There are two components for the Al_{2p} peaks (as discussed in Chapter 2, Section C-3): the one at the lower binding energy (73.0 eV) is characteristic of metallic Al, while the other one at the higher binding energy (76.2 eV) is assigned as AlO_x.

Table 3.2 shows the elemental composition and atomic ratios for samples A and B. Comparing the metallic percentages in these two samples, it is clear that more metallic Al is detected in sample B. From ADXPS (Chapter 2, Section C-5), an indication of the morphology of the carbon overlayer can be deduced by the n_o/n_s ratio. For sample A, the ratio of C to total Al content increases with decreasing take-off angle,

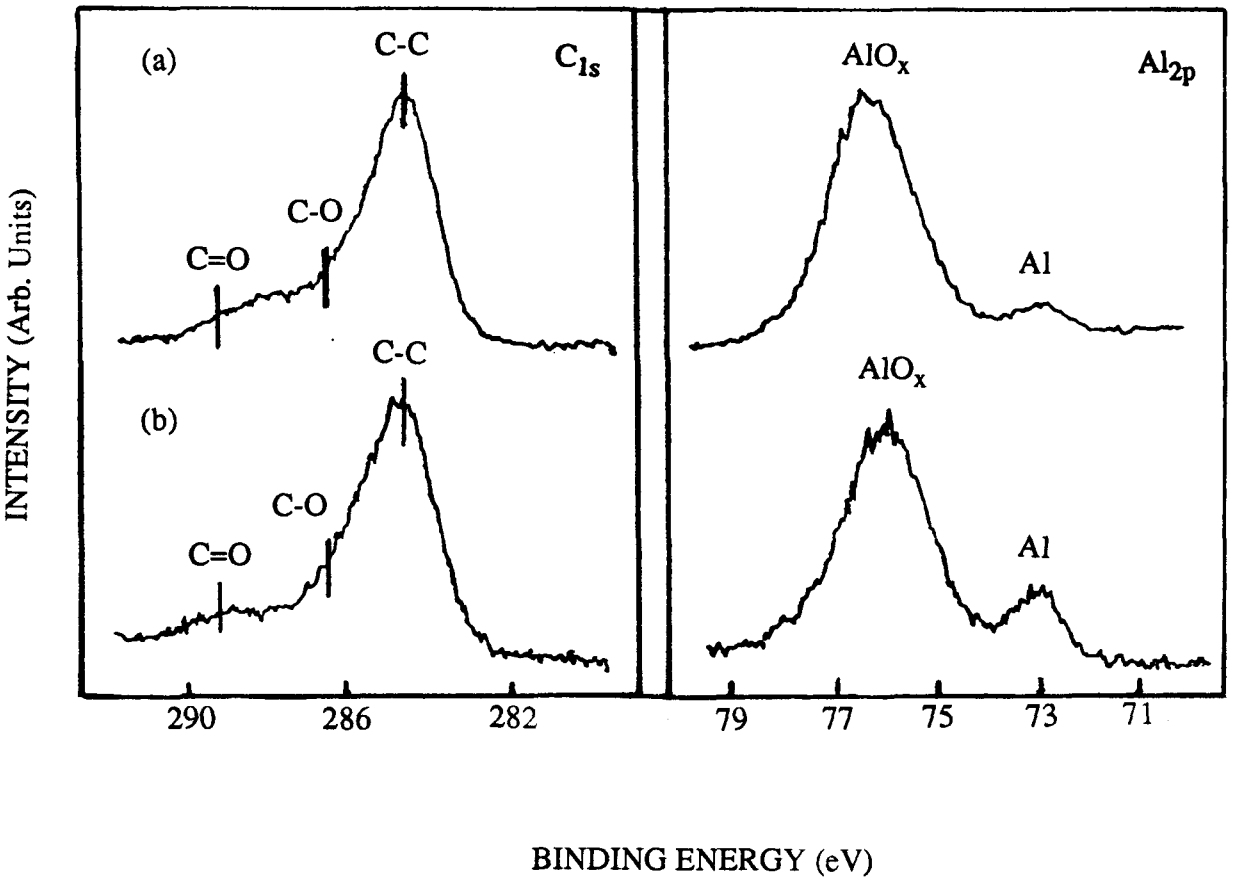

Figure 3.1 Narrow scan spectra of C_{1s} and Al_{2p} for (a) sample A (degreased Al) and (b) sample B (degreased and etched Al).

Table 3.2 Elemental composition and atomic ratios for degreased Al panel (sample A) and acid etched Al panel (sample B) with varying take-off angle, θ

Sample	θ(deg)	Elemental Composition (%)					Atomic Ratio
		O	C	*Al	AlO_x	**$Al_{(m)}$	C/Al
A	90	57.2	27.4	15.3	14.4	0.9	1.8
	45	51.6	35.2	13.2	13.0	0.2	2.7
	30	46.5	42.8	10.7	10.7	-	4.0
B	90	58.6	27.9	13.5	11.9	1.6	2.1
	45	59.9	26.3	13.8	13.2	0.6	1.9
	30	58.9	27.4	13.7	13.4	0.3	2.0

*Al indicates total Al content

**$Al_{(m)}$ indicates the metallic Al content

and this suggests that this sample has a continuous carbon layer on top of a continuous oxide layer, which itself adjoins the metallic aluminum. For sample B, by contrast, the C/Al ratio keeps basically constant with changing take-off angle. That suggests that the acid etched panel is not continuously covered by carbon, but instead has a patchy overlayer of carbon.

According to the XPS data, therefore, the chemically etched Al panel (sample B) has a different surface nature from that which is only degreased (sample A). The acidic etching seems to remove some oxide so that more metallic Al is exposed to the surface. Investigators reported [3.2] that this acidic etch treatment removes the weakly bound oxide, while a new and more strongly bound oxide layer is generated. By using electron microscopy, Chen et al. [3.3] suggested that when 2024-T6 Al alloy was subjected to the same acidic etching, a new layer of oxide, consisting of a network of shallow pores and protrusions or whiskers, was formed. Figure 3.2 respectively shows a high-resolution SEM micrograph for this etched Al panel and a deduced isometric drawing of the oxide morphology. It was concluded that these oxide whiskers should provide good mechanical interlocking for adhesion [3.4].

Some investigators have reported that the new oxide layer from the chemical etch treatment is amorphous AlO_x with varying quantities of adsorbed water and hydroxyl groups on the Al surface [3.5]. Although our XPS measurements cannot confirm that the oxide morphology in sample B is exactly the same as that obtained by Chen et al., our data does support the view that the acidic etched 7075-T6 Al surface provides some carbon-free AlO_x regions.

(a)

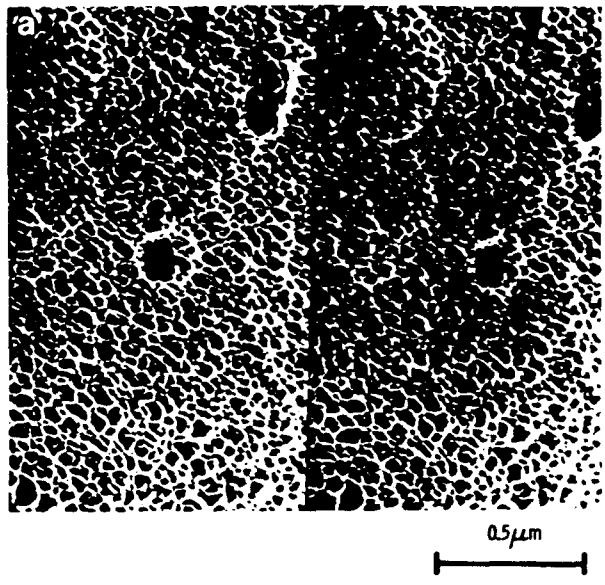

(b)

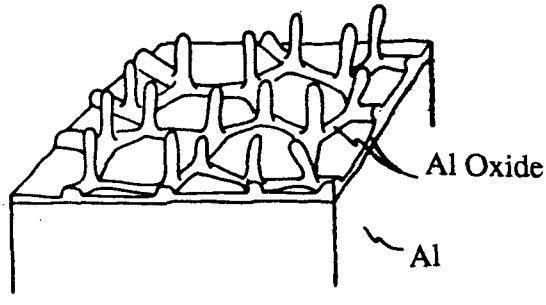

Figure 3.2 Acid etched 2024 Al surface (a) high resolution stereo electron micrograph; (b) form of surface according to ref. [3.3].

C-2. Polymerized γ-GPS Films

Sample C is a polymerized γ-GPS film deposited on a Al panel. Figure 3.3 provides a wide scan spectrum of it, and the photoemission peaks of O, C and Si are apparent. No Al signal is detected, and this indicates that the thickness of the silane film is greater than three times its IMFP. Both the binding energy of Si_{2p} (102.5 eV), and the difference between O_{1s} and Si_{2p} (430.4 eV) are consistent with the presence of Si-O-Si linkages [3.6]. Hence it is believed that a cross linkage silane network is formed.

The C_{1s} peak (Figure 3.4a) contains C-O (286.6 eV) and C-C (285.0 eV) components. The C-O component is mainly contributed by the C-O and epoxy groups of γ-GPS, while the C-C component originates from the hydrocarbon chains. As stated before (Chapter 2, Section B-2), other investigators have suggested that because of different degrees of polymerization, the silane films may contain Si-O-Si, Si-OH, or Si-O-C [1.21, 1.22], and it is not easy to distinguish each by XPS through the Si_{2p} peak [3.7]. In addition O_{1s} does not give useful information since O signals can arise from many sources (including impurities). Therefore no analyzing for these two photoemission peaks was performed.

Table 3.3 records the elemental composition and atomic ratios for samples C and D (water rinsed sample C). For sample C, the ratio of C-C to Si indicates that the C-C chains are randomly oriented. Also the C-O/Si ratio increases as θ decreases. That suggests that the C-O group and the epoxy group are preferentially oriented toward the surface. For sample D, after rinsing with deionized water, the ratios C-O/C-C and C-O/Si reflect the decrease of C-O groups on the polymer surface. A possible explanation is that during the rinsing procedure, some unhydrolyzed methoxyl groups

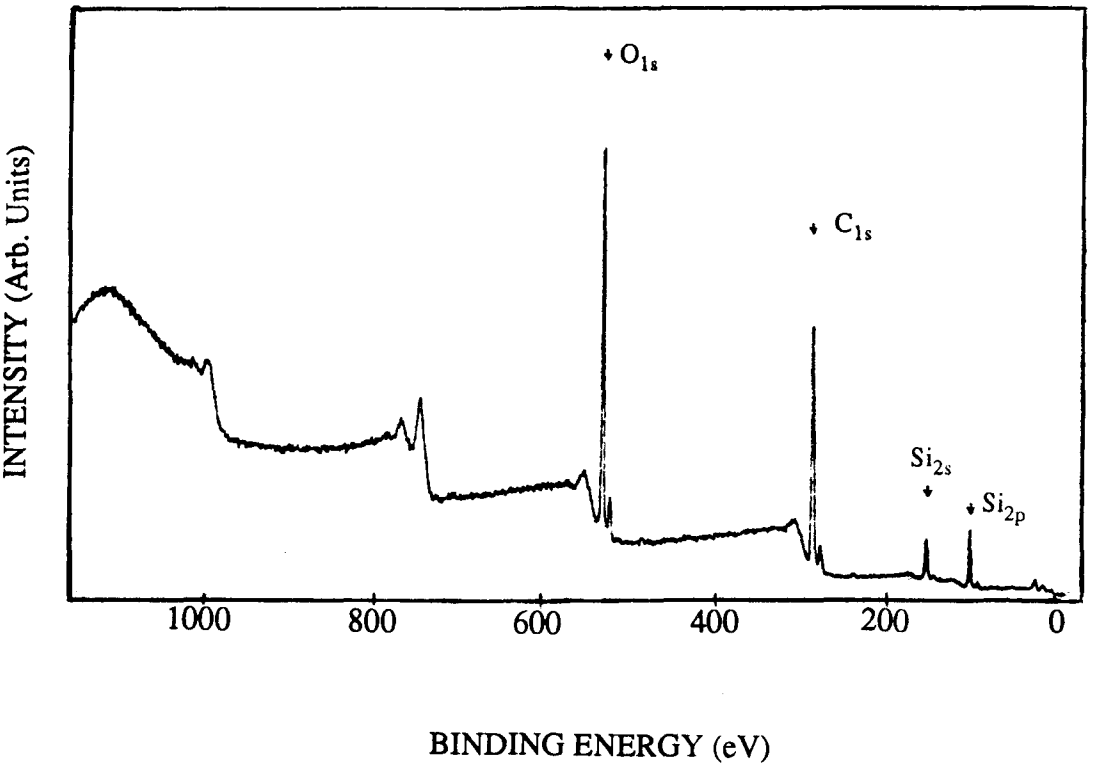

Figure 3.3 Wide scan spectrum for sample C, the polymerized γ-GPS film.

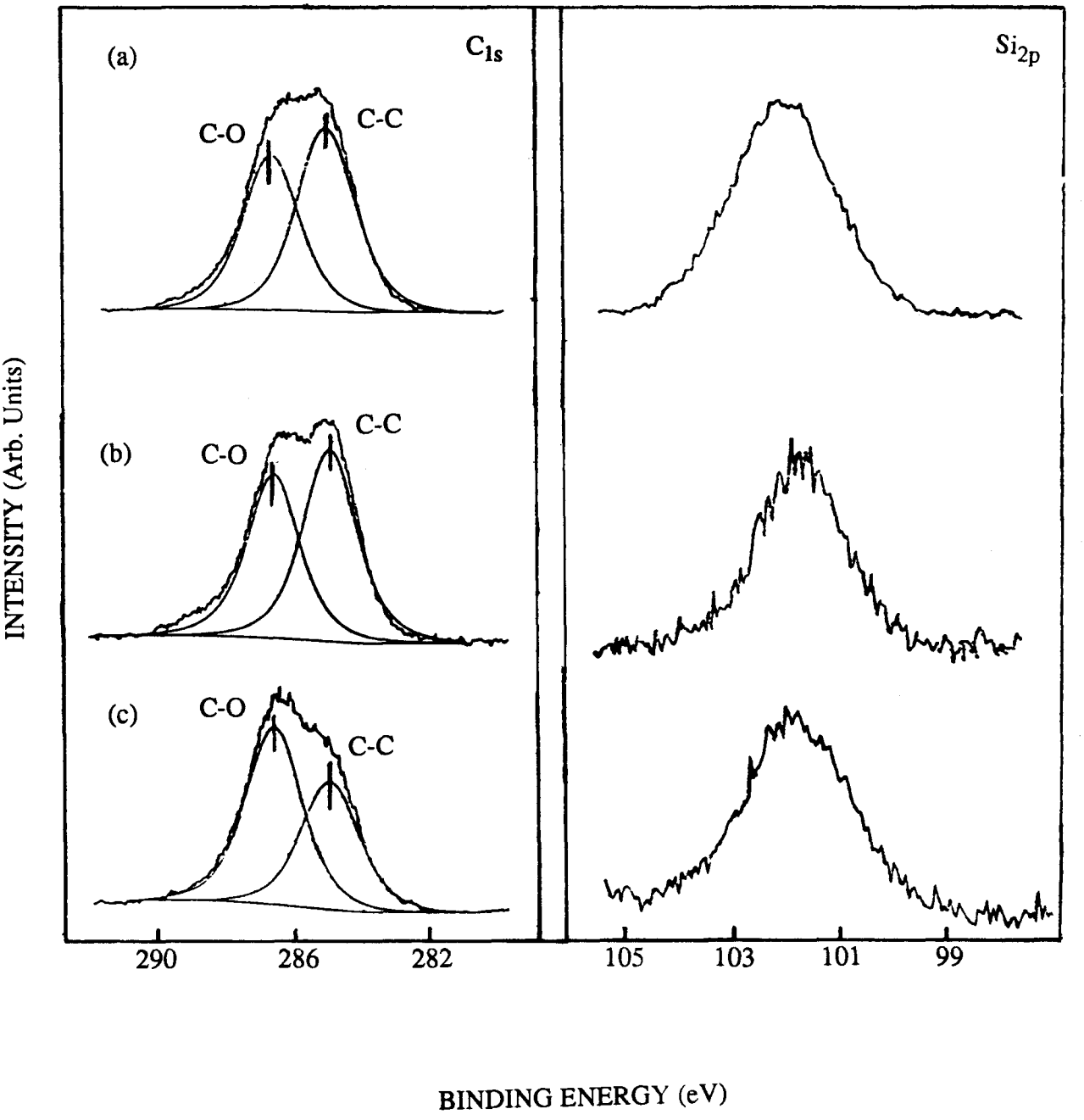

Figure 3.4 The C_{1s} and Si_{2p} narrow scan spectra for (a) sample C, a polymerized γ-GPS film, (b) sample E, a γ-GPS/degreased Al interface, and (c) sample F, a γ-GPS/etched Al interface.

Table 3.3 Elemental composition and atomic ratios for polymerized γ-GPS film (sample C) and water rinsed γ-GPS polymer film (sample D)with varying take-off angle, θ

Sample	θ (deg)	Elemental Composition (%)					Atomic Ratio		
		O	C	Si	C-O	C-C	$\frac{\text{C-O}}{\text{C-C}}$	$\frac{\text{C-O}}{\text{Si}}$	$\frac{\text{C-C}}{\text{Si}}$
C	90	42.8	50.7	6.5	23.2	27.5	0.8	3.6	4.3
	60	42.9	51.1	6.0	26.8	24.1	1.1	4.4	4.0
	45	43.6	50.5	5.9	28.0	22.5	1.3	4.7	3.6
	30	41.7	52.8	5.5	29.1	23.7	1.2	5.3	4.3
D	90	43.5	50.4	6.1	23.5	26.9	0.87	3.9	4.4
	45	41.8	51.6	6.6	20.3	31.8	0.64	3.1	4.7
	30	41.9	51.9	6.3	21.9	30.0	0.73	3.5	4.8

undergo hydrolysis (i.e. $\equiv Si\text{-}OCH_3 + H_2O \rightarrow \equiv Si\text{-}OH$) so that the concentration of C-O groups decreases.

C-3. γ-GPS/Al Interfaces

Figures 3.5 and 3.6 represent the wide scan spectra for sample E (γ-GPS/degreased Al) and sample F (γ-GPS/etched Al) respectively. Photoemission peaks of O, C, Si and Al are seen from both samples. Figures 3.4b and c give narrow scan spectra for C_{1s} and Si_{2p} peaks; comparing samples C, E, and F, the Si_{2p} peaks cannot provide any direct evidence for the Al-O-Si chemical bonding. Table 3.4 tabulates the elemental compositions and atomic ratios. For sample E, the increase of Si to Al ratio with decreasing θ suggests a continuous overlayer film is formed by γ-GPS, that is the carbon coated degreased Al panel is itself covered by a continuous layer of silane. For sample F, in contrast, the random ratio of Si/Al with decreasing θ (increasing surface sensitivity) suggests that the silane overlayer has a patchy form.

Atomic ratios can provide some orientation information for groups in the silane overlayer. Sample E has a continuous overlayer model, therefore, the increase of the C-O/Al and C-C/Al ratios with decreasing θ reflects that both the C-O and C-C groups orient towards the surface (i.e. away from the interface). However, because of the patchy overlayer in sample F, the C-O/Al and C-C/Al ratios cannot provide much useful information on orientation.

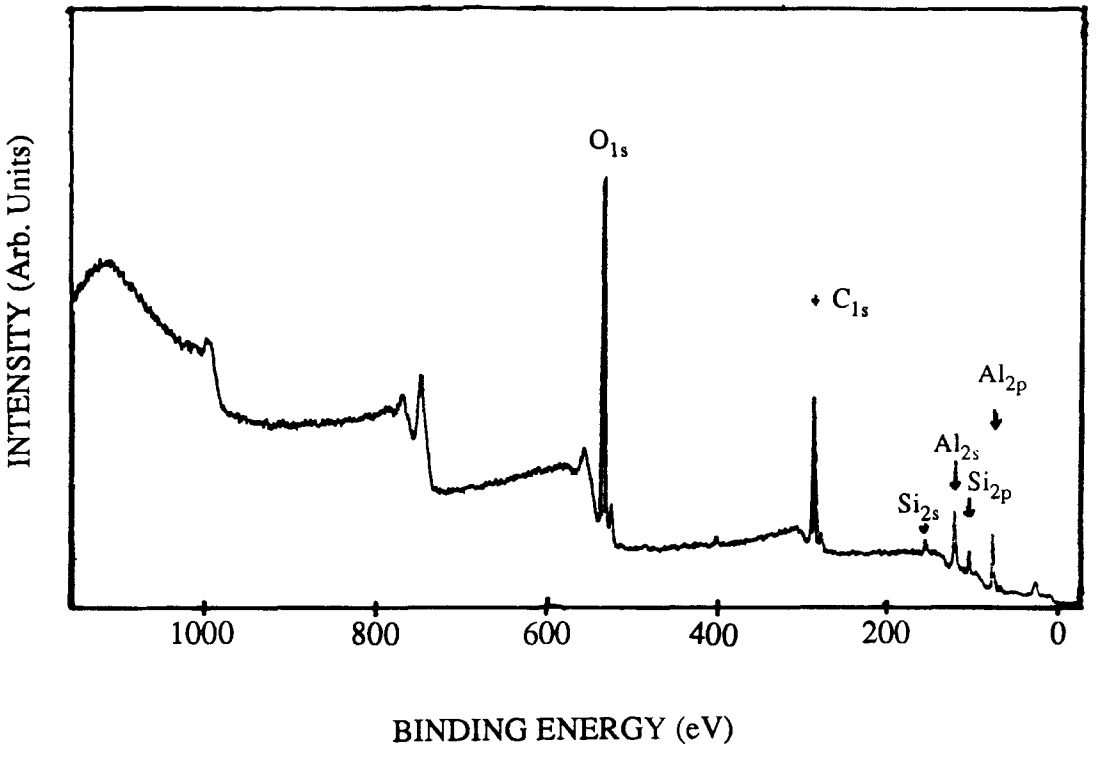

Figure 3.5 A wide scan XPS spectrum for a γ-GPS/degreased Al interface (sample E).

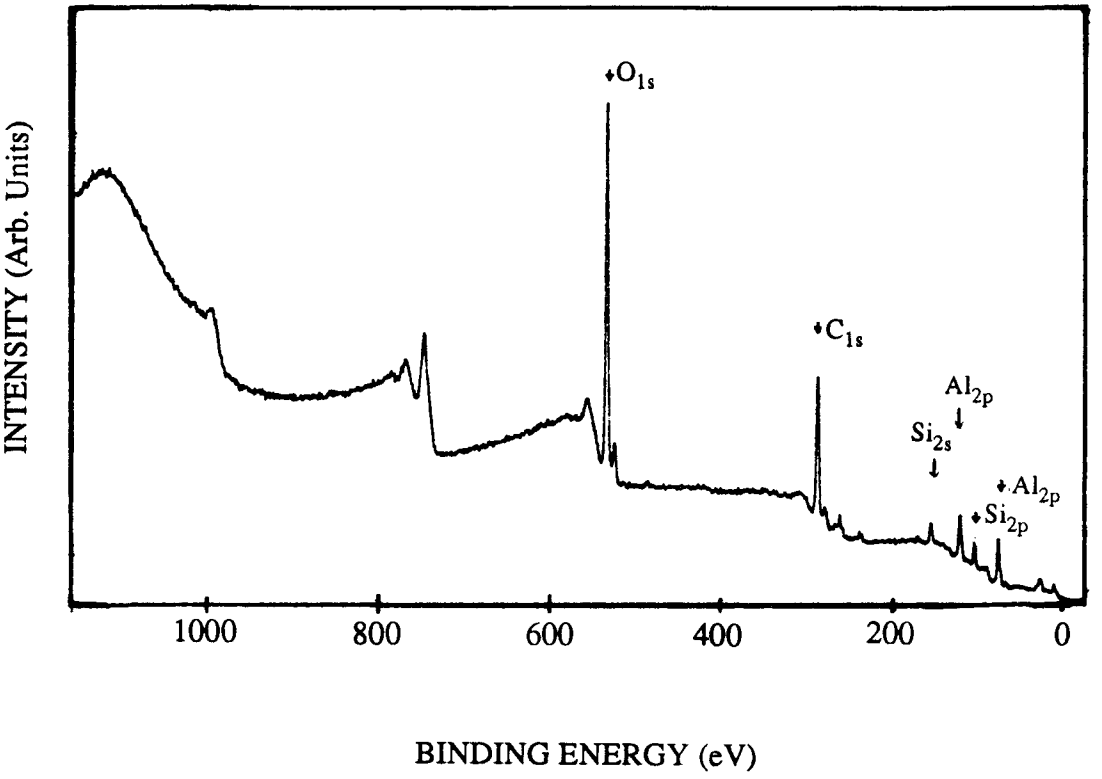

Figure 3.6 A wide scan XPS spectrum for a γ-GPS/etched Al interface (sampleF).

Table 3.4 Elemental composition and atomic ratios for γ-GPS/degreased Al (sample E) and γ-GPS/etched Al (sample F) with varying take-off angle, θ

Sample	θ (deg)	Elemental Composition (%)					
		O	**C	Si	*Al	C-O	C-C
E	90	53.0	33.1	1.7	12.2	15.2	17.9
	60	50.3	36.3	3.3	10.1	14.3	22.0
	45	48.3	39.8	3.0	9.0	14.0	25.7
	30	41.6	48.2	4.1	6.1	15.6	32.6
F	90	53.7	32.6	3.4	10.3	18.9	13.7
	60	53.6	35.4	3.0	8.0	17.9	17.5
	45	52.1	37.0	3.8	7.1	17.1	19.9
	30	54.9	33.1	3.8	8.2	13.9	19.2

		Atomic Ratio				
		$\frac{Si}{Al}$	$\frac{C}{Al}$	$\frac{C\text{-}O}{Al}$	$\frac{C\text{-}C}{Al}$	$\frac{C\text{-}O}{C\text{-}C}$
E	90	0.14	2.7	1.3	1.5	0.85
	60	0.33	3.6	1.4	2.2	0.65
	45	0.33	4.4	1.6	2.9	0.54
	30	0.67	7.9	2.6	5.3	0.49
F	90	0.33	3.2	1.8	1.3	1.4
	60	0.37	4.4	2.2	2.2	1.0
	45	0.53	5.2	2.4	2.8	0.86
	60	0.46	4.0	1.7	2.4	0.72

* Al indicates total Al content.

** C indicates total C content.

C-4. γ-APS/Al Interfaces

Figures 3.7 and 3.8 show the wide scan spectra for sample G (γ-APS/Al interface at pH = 3.0) and sample H (γ-APS interface at pH=10.4). Photoemission peaks of O, N, C, Si and Al are detected in both interfaces, while a Cl peak is also observed in sample G (this arose from the addition of HCl). Figure 3.16 gives their narrow scan spectra of the Al_{2p} peaks; in both these cases, the Al_{2p} peaks correspond to oxide only. The Al_{2p} peak (at 76.2 eV) in sample C is consistent with that observed for the γ-GPS/Al interface, whilst in sample H, the Al_{2p} peak appears at the slightly lower binding energy of 75.5 eV. This suggests that the surface character is different when the deposition is made in an alkaline medium; indeed the observed binding energy would appear consistent with the formation of $Al(OH)_y$ [3.8]. Boerio et al. observed a similar result [3.9]. These authors reported that in basic solution of γ-APES, the oxidized surface of 2024 Al was rapidly etched and also that the etching rate decreased as the solution pH was decreased.

Table 3.5 records elemental composition and atomic ratios against take-off angle for samples G and H. The almost constant Si/Al ratio observed from sample G suggests that the γ-APS forms a patchy overlayer in acid medium (pH=3.0). By contrast, the increase in the Si/Al ratio with increasing surface sensitivity is consistent with expectation for a continuous silane overlayer.

Normally the C_{1s} and O_{1s} peaks contain contributions of contamination, but the N_{1s} peaks almost totally originate only from the γ-APS; thus N_{1s} can provide extra structural information for these silane films. Chiang et al. suggested that the $-NH_2$ groups of aminosilanes hydrolyze in water to give two structural forms in equilibrium

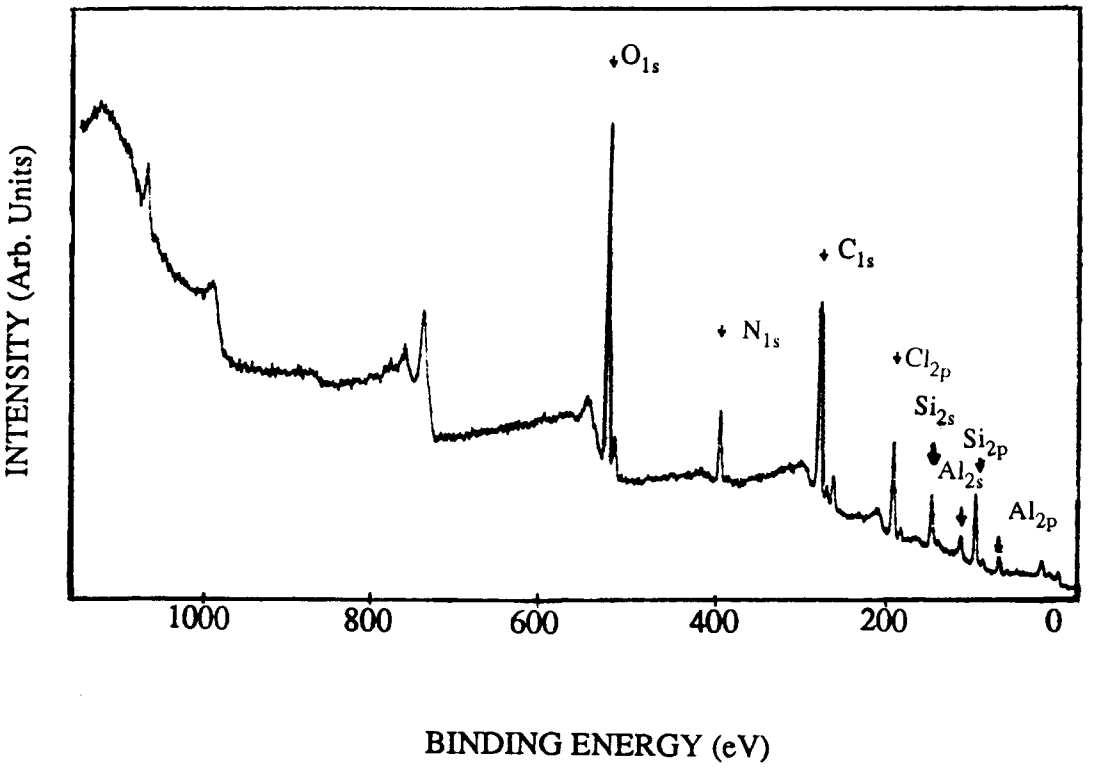

Figure 3.7 A wide scan XPS spectrum for a γ-APS/etched Al interface at pH=3.0 (sample G).

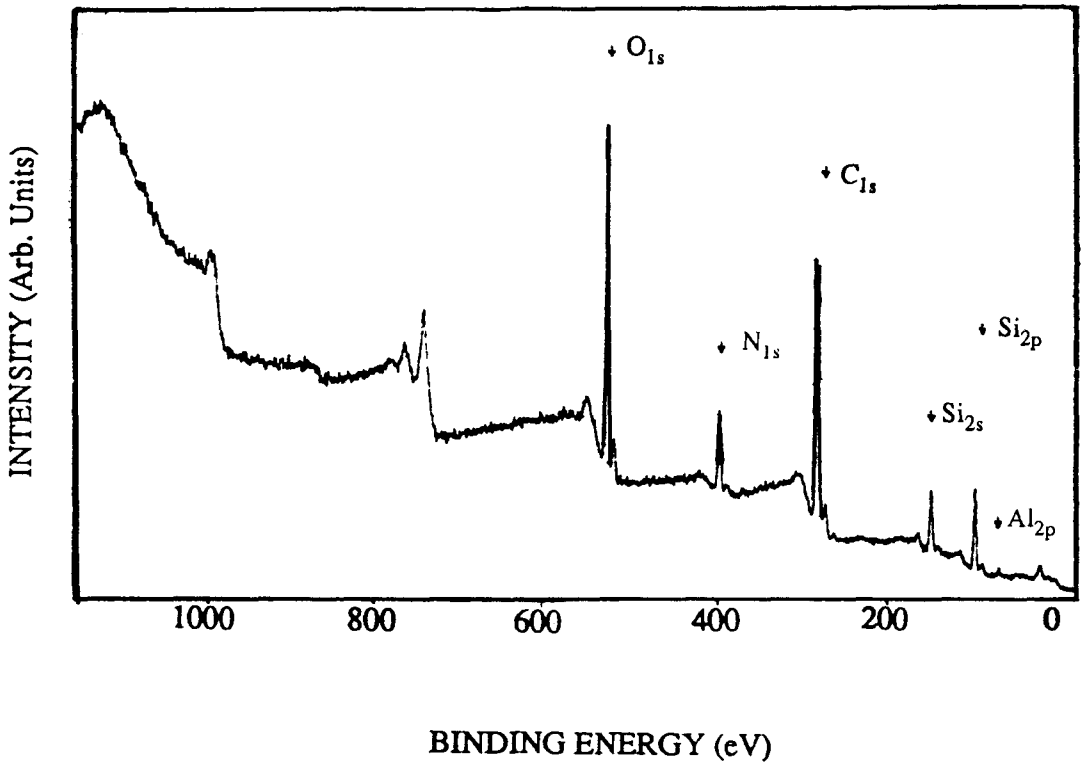

Figure 3.8 A wide scan XPS spectrum for a γ-APS/etched Al interface at pH=10.4 (sample H).

Table 3.5 Elemental composition and atomic ratios for γ-APS/etched Al at pH=3.0 (sample G) and γ-APS/etched Al at pH=10.4 (sample H) with varying take-off angle, θ

Sample	θ (deg)	Elemental Composition (%)								
		O	N	N_1	N_2	N_3	C	Cl	Si	Al
G	90	33.4	9.4	6.0	2.5	0.9	39.2	5.1	8.8	4.1
	45	33.1	7.8	3.3	2.9	1.6	41.7	4.1	8.9	4.4
	30	32.9	8.4	3.4	3.4	1.6	42.3	3.8	8.4	4.2
	20	31.2	7.2	2.4	3.1	1.7	45.8	3.0	8.1	4.6
H	90	30.7	10.6	1.5	3.8	5.4	47.3	-	9.6	1.9
	45	29.3	9.4	0.8	4.0	4.7	50.5	-	9.2	1.6
	30	28.0	8.7	0	4.5	4.2	52.9	-	9.2	1.3
	20	26.2	7.2	0	3.5	3.7	55.4	-	9.9	1.3

		$\frac{Si}{Al}$	$\frac{C}{N}$	$\frac{N_1}{N}$	$\frac{N_2}{N}$	$\frac{N_3}{N}$
G	90	2.1	9.6	0.64	0.27	0.10
	45	2.0	9.5	0.42	0.37	0.21
	30	2.0	10.0	0.40	0.40	0.20
	20	1.8	10.0	0.33	0.43	0.24

		$\frac{Si}{Al}$	$\frac{C}{Al}$	$\frac{N_1}{Al}$	$\frac{N_2}{Al}$	$\frac{N_3}{Al}$	$\frac{N_1}{Si}$	$\frac{N_2}{Si}$	$\frac{N_3}{Si}$
H	90	5.1	24.9	0.79	2.0	2.8	0.16	0.39	0.56
	45	5.8	31.6	0.48	2.5	2.9	0.08	0.44	0.50
	30	7.1	40.7	0	3.5	3.2	0	0.49	0.46
	20	7.6	42.6	0	2.7	2.8	0	0.36	0.37

[1.23, 3.10]. One is an open, extended non-ring structure and the other is a cyclic H-bonded amine structure (≡Si-OH···NH_2).

However, in earlier studies, the assignment of N_{1s} components is not consistent. Most investigators assigned two components for the N_{1s} peak [3.11-3.13]: one being the extended non-ring structure, the other the ≡Si-O^-···NH_3^+ structure. Further the binding energies of these two components are varied from different authors. In our work, we believe that three kinds of nitrogen coexist: acid protonated (≡Si$(CH_2)_3NH_3^+$), H-bonded (≡Si-OH···NH_2), and free NH_2 (≡Si$(CH_2)_3NH_2$) groups. In the N_{1s} peak curve analysis, therefore, three components are assigned. Based upon the N_{1s} assignment of Boerio et al [1.27], the components of N_{1s} peaks with their corresponding binding energies are shown in Figure 3.9. The first component, N_1, at 401.9 eV, is attributed to the acidic protonated form. The second component, N_2 at 400.7 eV, is assigned as the H-bonded form, and the third component N_3 with binding energy 399.5 eV represents the free form.

For sample G, the patchy silane overlayer limits the possibilities for atomic ratios to provide orientation information, although individual ratios of N_1, N_2 and N_3 to total nitrogen content (N) can give some indications of the distribution of the amino groups. From Table 3.5, the N_1 to N ratio increases with decreasing θ. That suggests -NH_3^+ prefers to stay close to the interface. On the other hand, N_2/N and N_3/N change randomly as the take-off angle varies, and it is accordingly concluded that N_2 and N_3 orient randomly with respect to the mean of the total N distribution.

Since sample H has a continuous silane overlayer, the N to Al ratios are valuable for interpreting the orientation of the amino groups. The N_1/Al ratio falls to zero at θ=30°; it suggests -NH_3^+ still stays close to the interface, as in acidic solution (although

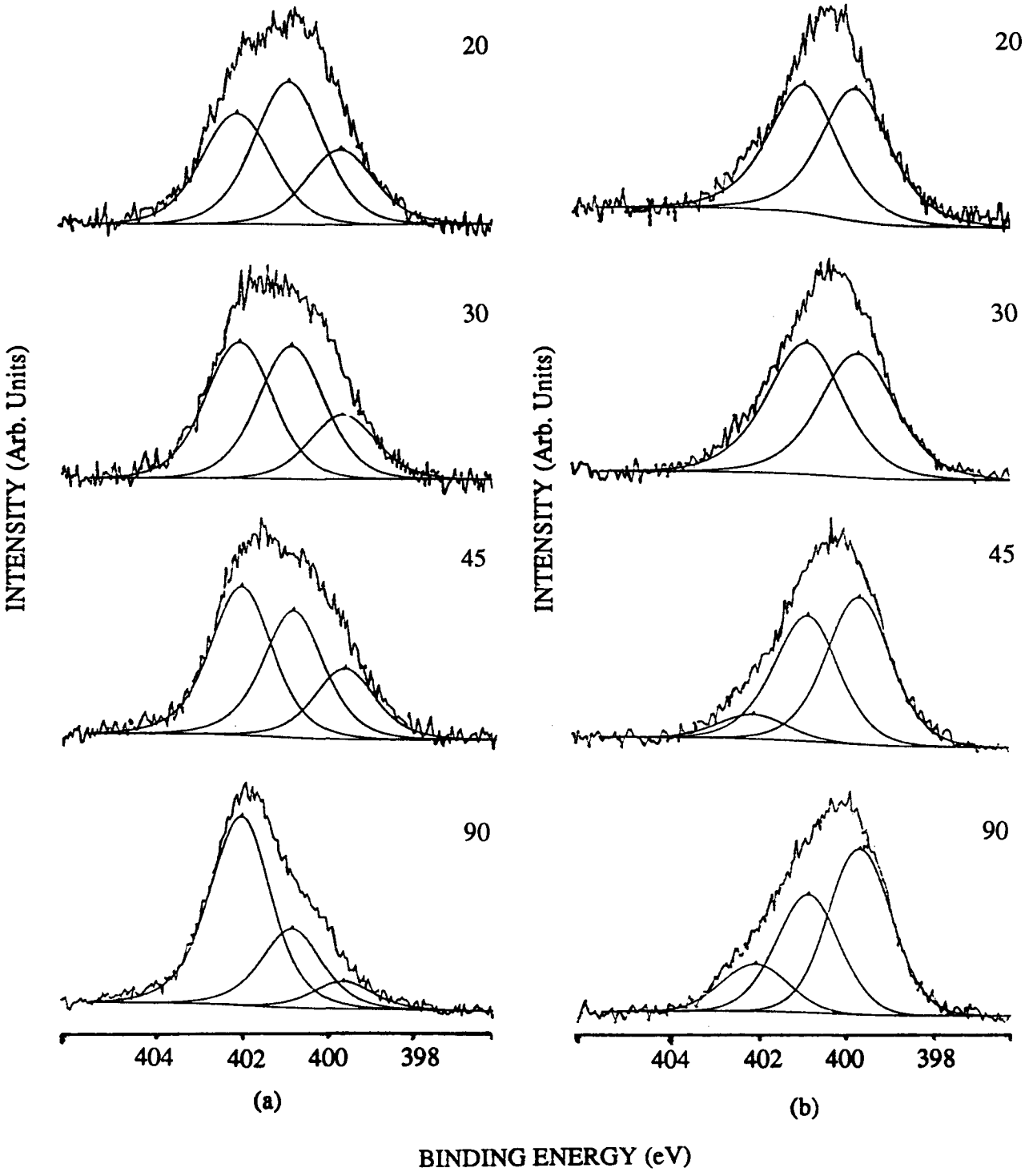

Figure 3.9 N_{1s} spectra for take-off angle varying from 90^{o} to 20^{o} for (a) sample G and (b) sample H.

now the total amount of NH_3^+ is much less). The angular dependence of the N_2/Al ratio, and the constant N_2/Si ratio, implies N_2 remains close with Si on the surface. The N_2 component may involve contributions from intramolecularly H-bonded amino groups. The N_3/Al ratios suggest free -NH_2 groups orient randomly in the silane overlayer.

Figure 3.10 shows the two molecular film structures proposed for samples G and H. In summary, most -NH_2 groups in acidic γ-APS are in the -NH_3^+ structural form. These -NH_3^+ groups stay close to the interface, while the rest of the -NH_2 groups either intermolecularly hydrogen bond with Al-OH or stay free in the silane overlayer. By contrast, in sample H, only a small proportion of the -NH_2 groups are present in the NH_3^+ form which concentrates near to the interface. Most -NH_2 groups H-bond intramolecularly with ≡Si-OH groups and form a continuous layer of silane film on the Al surface. Both these two cases indicate quite low probabilities for direct approach between ≡Si-OH on the silane and Al-OH on the metallic surface.

Boerio and Williams [1.26] reported that γ-APES has a higher degree of polymerization on iron in acidic solution than in alkaline solution. They suggested a molecular structure at pH=8.0 in which γ-APES is "right side up" (Figure 3.11a), that is the ≡Si-OH bond with surface Al-OH groups, and the -NH_3^+ groups orient towards the surface. For alkaline deposition, on the other hand, γ-APES, has the "upside down" structure (Figure 3.11b) in which -NH_2 groups stay near the interface. Our suggested structures are different from those of Boerio et al.. However, it is necessary to point out that their conclusion was deduced from a corrosion study, rather than direct structural study. Secondly, the materials used are different in the two studies.

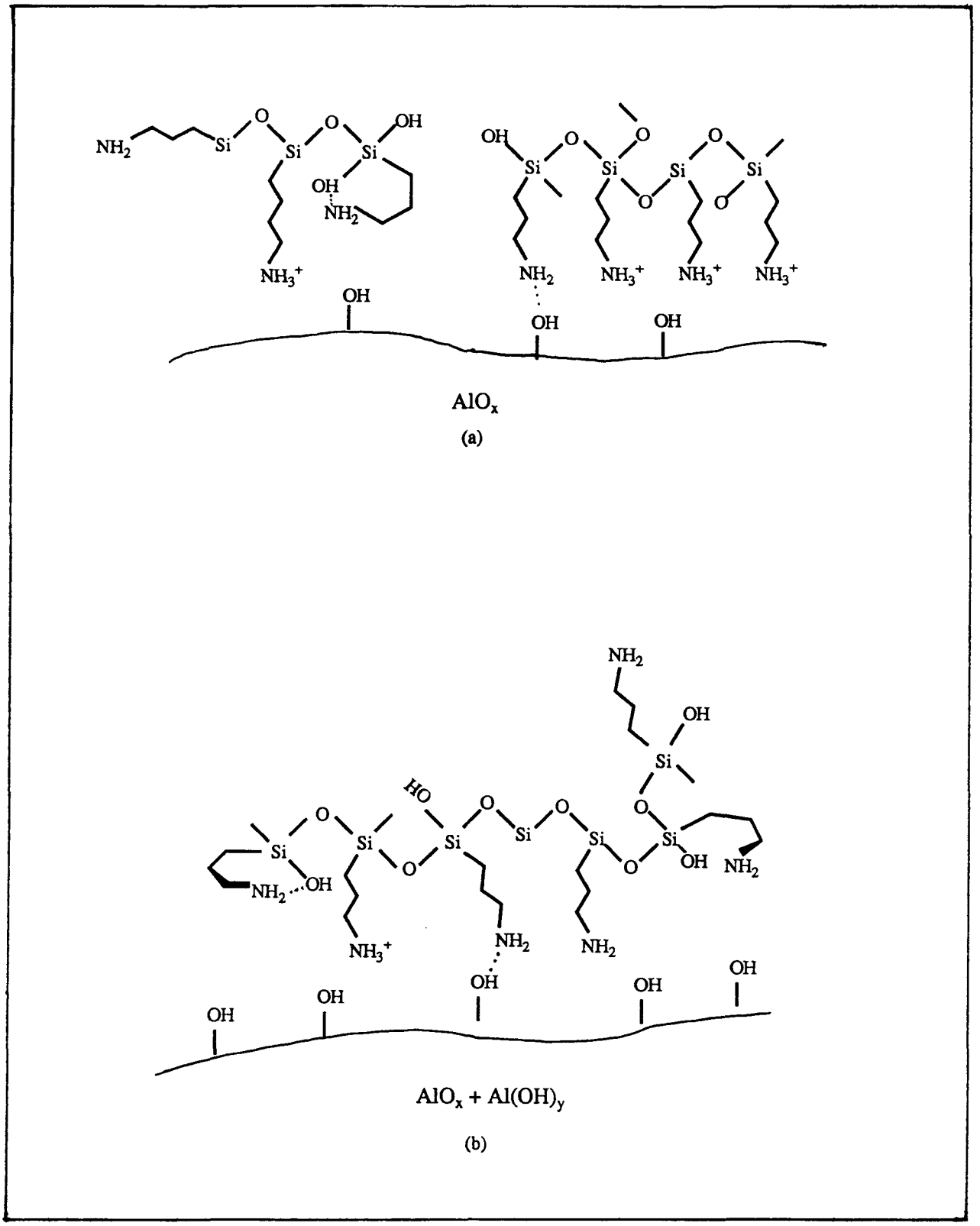

Figure 3.10 A suggested film structure of γ-APS deposited on Al at (a) pH=3.0; (b) pH=10.4.

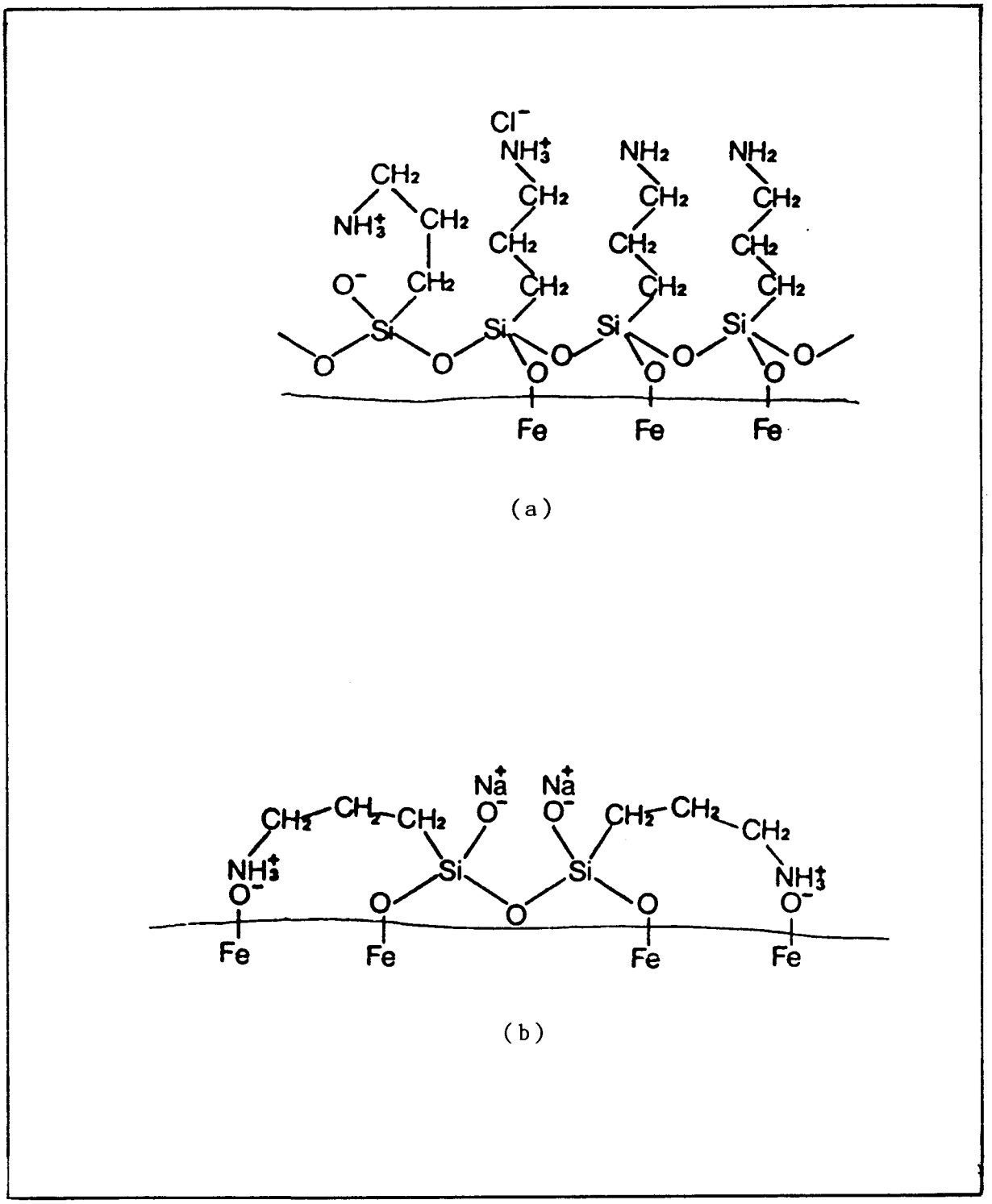

Figure 3.11 Structure of γ-APES films deposited on iron according to Boerio et al. [1.26]: (a) pH=8.0 and (b) pH=12.0.

C-5. γ-MGPS/Al Interface

Figure 3.12 shows a wide scan spectrum of the γ-MGPS/Al interface (sample I) after being held under vacuum overnight; photoemission peaks of Al, Si, S, C, and O are detected. Table 3.6 tabulates the elemental concentration and atomic composition ratios. During the preparation of the γ-MGPS solution, it was found that γ-MGPS is not very miscible with the methanol/ distilled water solution. It took about 30 min to get a homogeneous solution. Thus the contribution of the C-O signal may arise from unhydrolyzed methoxyl groups. The constant ratio of Si to Al at varying θ indicates the patchy silane overlayer is formed. Although γ-MGPS has a tag functional group, -SH, the patchy property limits the ability of atomic ratios to give orientation information.

Under X-ray irradiation, polymers have occasionally been observed to degrade during XPS analysis. This phenomenon was also seen in sample I, where an initial study on a freshly prepared sample showed an abnormal behavior, specifically that the amount of Al appeared to increase as the take-off angle decreased. This behavior is abnormal since according to the basics of ADXPS (Chapter 2, SectionC-5), the intensity of the substrate should either keep constant or decrease with reducing θ for the four models mentioned in Figure 2.10 (other results observed in this research agree with these basic principles). That suggests that the γ-MGPS overlayer degrades in the presence of the X-ray radiation (or simply under vacuum). As stated above, the data in Table 3.6 were obtained after sitting overnight in the analysis chamber. Comparing with the initial (beam affected) measurements, the peak positions and the peak shapes of the individual photoemission peaks do not change. This degradation possibly arises from the short curing time for the deposition.

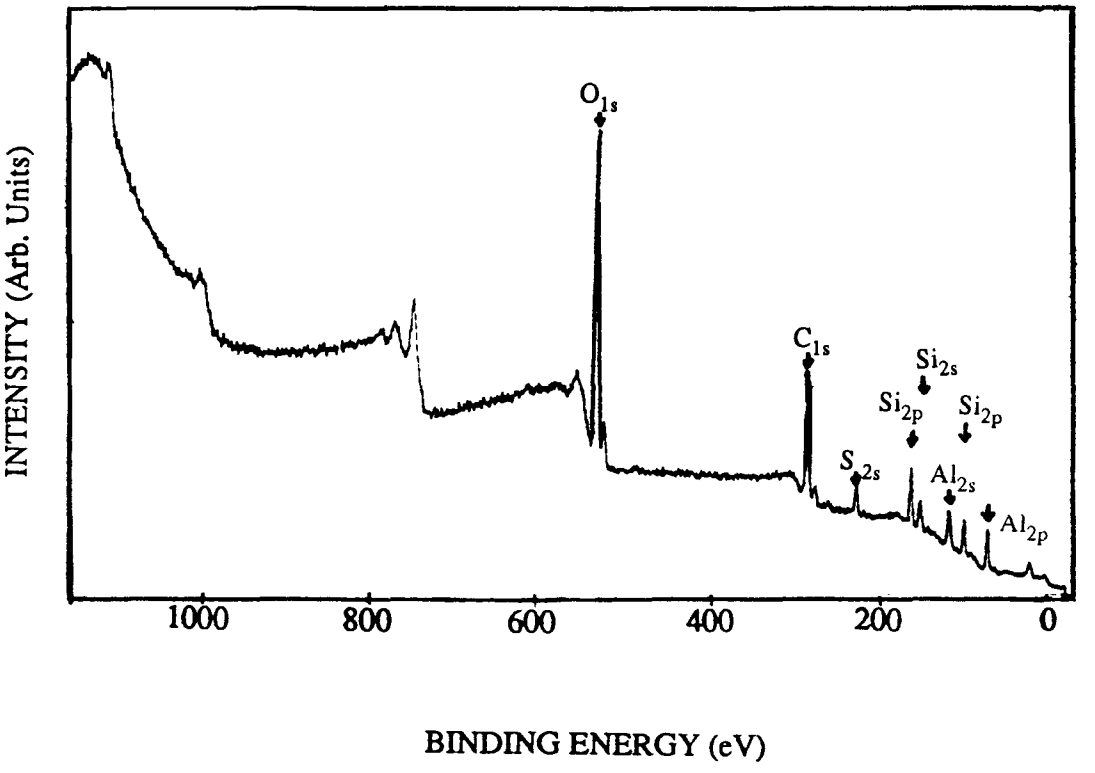

Figure 3.12 A wide scan XPS spectrum for a γ-MGPS/etched Al interface (sample I).

Table 3.6 Elemental composition and atomic ratios for γ-MGPS/etched Al (sample I) with varying take-off angle, θ

Sample	θ (deg)	Elemental Composition (%)							Atomic Ratio
		O	C	S	Si	*Al	AlO_x	$Al_{(m)}$	Si/Al
I	90	46.0	29.6	3.7	6.8	13.9	13.3	0.6	0.49
	45	45.3	30.2	3.6	7.4	13.6	13.3	0.3	0.54
	30	47.1	29.8	3.5	6.6	13.0	13.0	0	0.50
	20	48.7	27.8	2.9	5.4	15.2	15.2	0	0.36

*Al indicates total Al content

C-6. Biased Silane/Al Interfaces

Regular angle dependent XPS measurements of Al_{2p} peaks (Figures 3.13a - 3.16a) for samples E to I seem unable to get any direct evidence for the existence of Al-O-Si bonding, but following the proposal of Pertsin and Pashunin [1.36] we were interested in investigating whether more information could be obtained with the bias potential technique. Therefore, a negative potential is applied to each of these interfaces. Figure 3.13 compares the biased and non-biased Al_{2p} spectra of the γ-GPS/degreased Al interface (sample E). Neither the peak shape nor position changes under the bias potential. All AlO_x peaks are shifted exactly by -93 eV in the bias process. According to the background stated in Chapter 1, Section C, the steady surface potential, φ_s, of sample E is exactly equal to φ_h. That suggests all the Al atoms in AlO_x have identical electrical properties. Therefore, it appears that γ-GPS has no direct interaction with the degreased Al panel.

Figure 3.14 shows the biased and non-biased Al_{2p} spectra for sample F (γ-GPS/etched Al interface). Now an extra peak appears at a higher binding energy than that for the original AlO_x. At small θ, the intensity is more prominent. This result suggests that some AlO_x in this interface have different electrical properties (i.e. φ_s) from the rest of the AlO_x. We postulate that some AlO_x may interact with the γ-GPS to form Al-O-Si bonding in the interface. This interaction may change the electrical conductivity of that region, and lead to a different f factor. The increase in the extra peak in Figure 3.15, with decreasing θ, suggests that it is the uppermost part of the metal oxide which is affected. It is definitely the AlO_x which is affected, since the Al metallic peak in sample F is not affected by the differential charging effect.

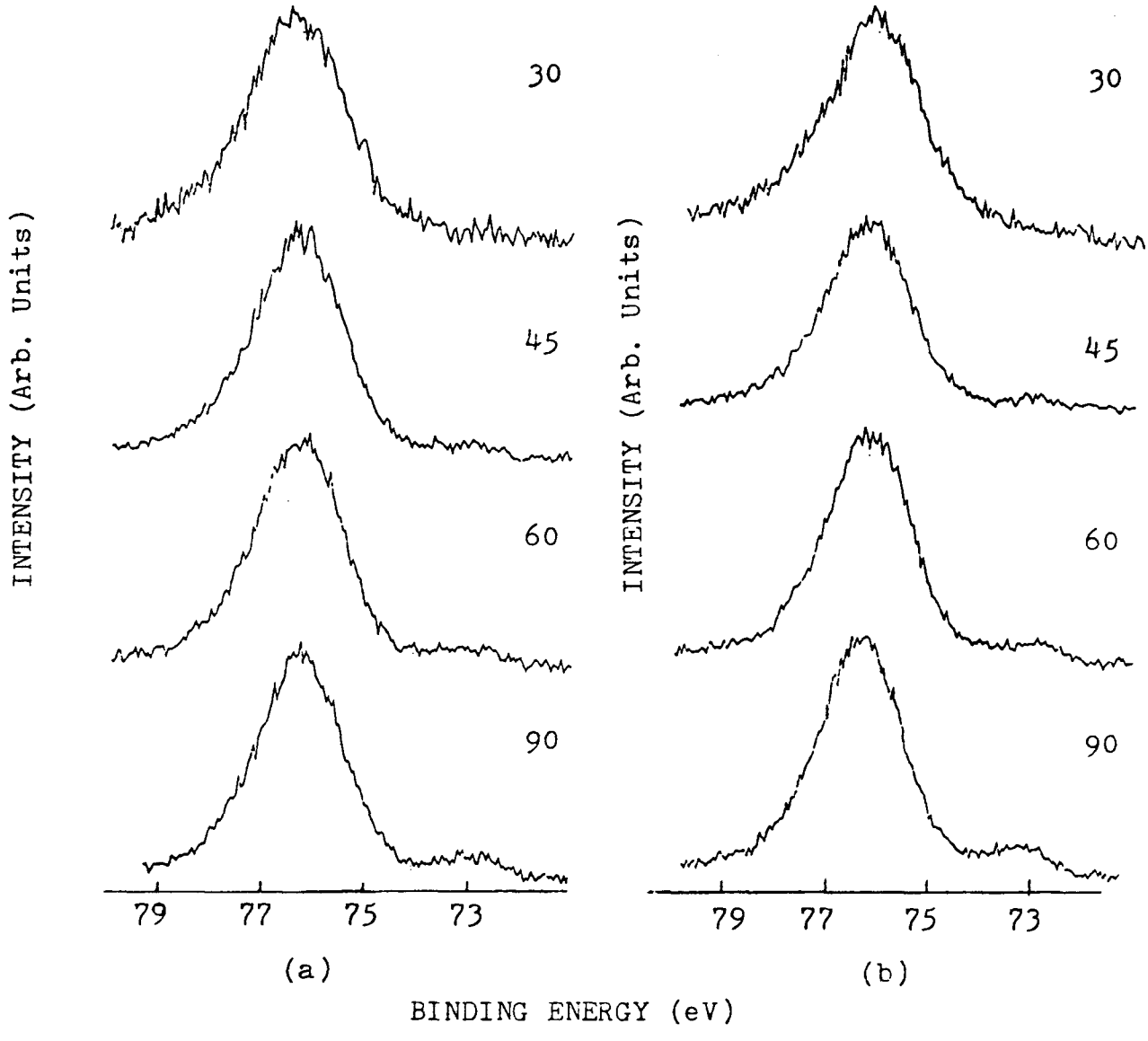

Figure 3.13 Al_{2p} spectra with varying take-off angles from 90^{o} to 30^{o} for (a) sample E (γ-GPS/degreased Al interface) not biased and (b) sample E biased.

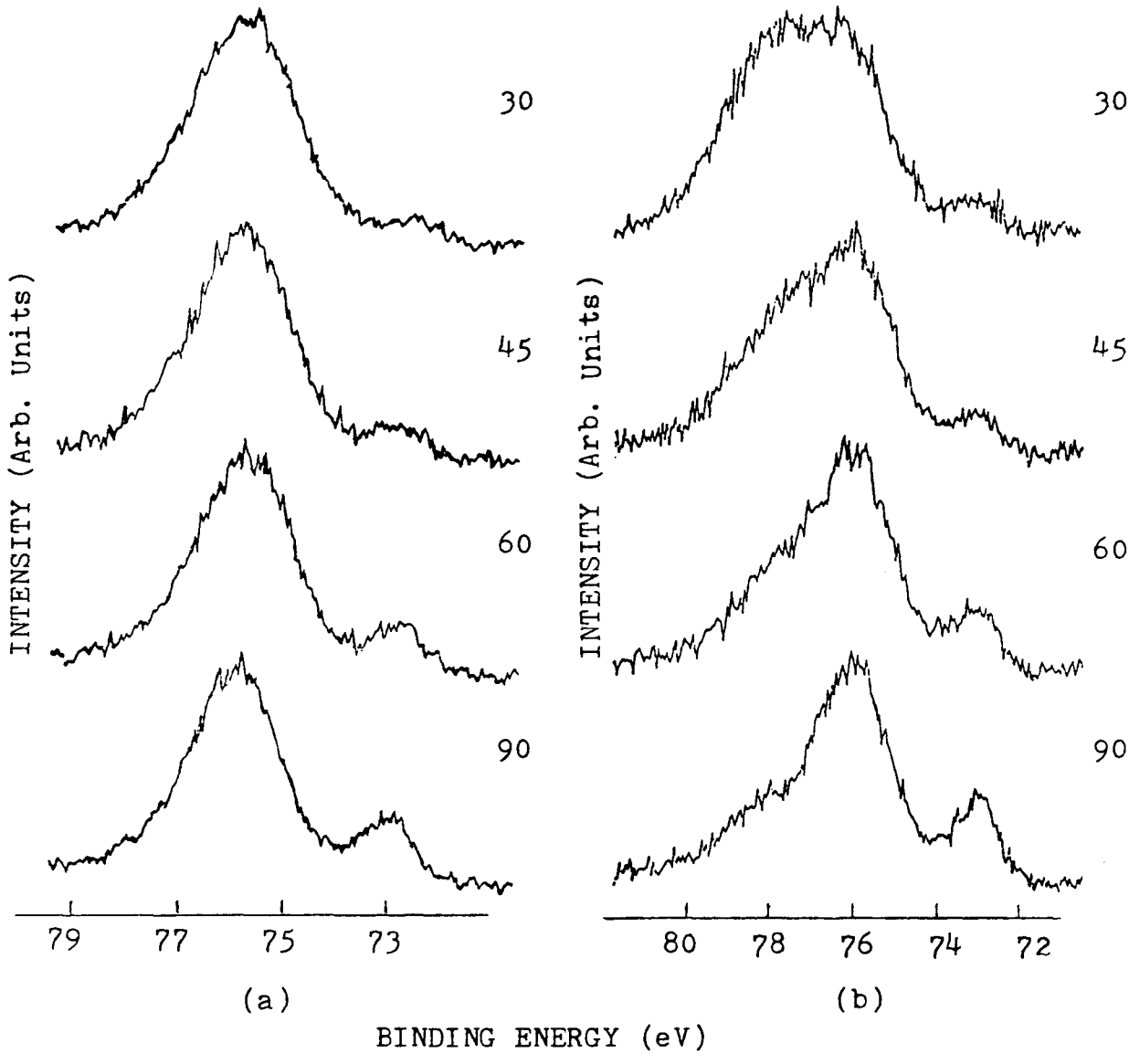

Figure 3.14 Al_{2p} spectra with varying take-off angles from 90^{o} to 30^{o} for (a) sample F (γ-GPS/etched Al interface) not biased and (b) sample F biased.

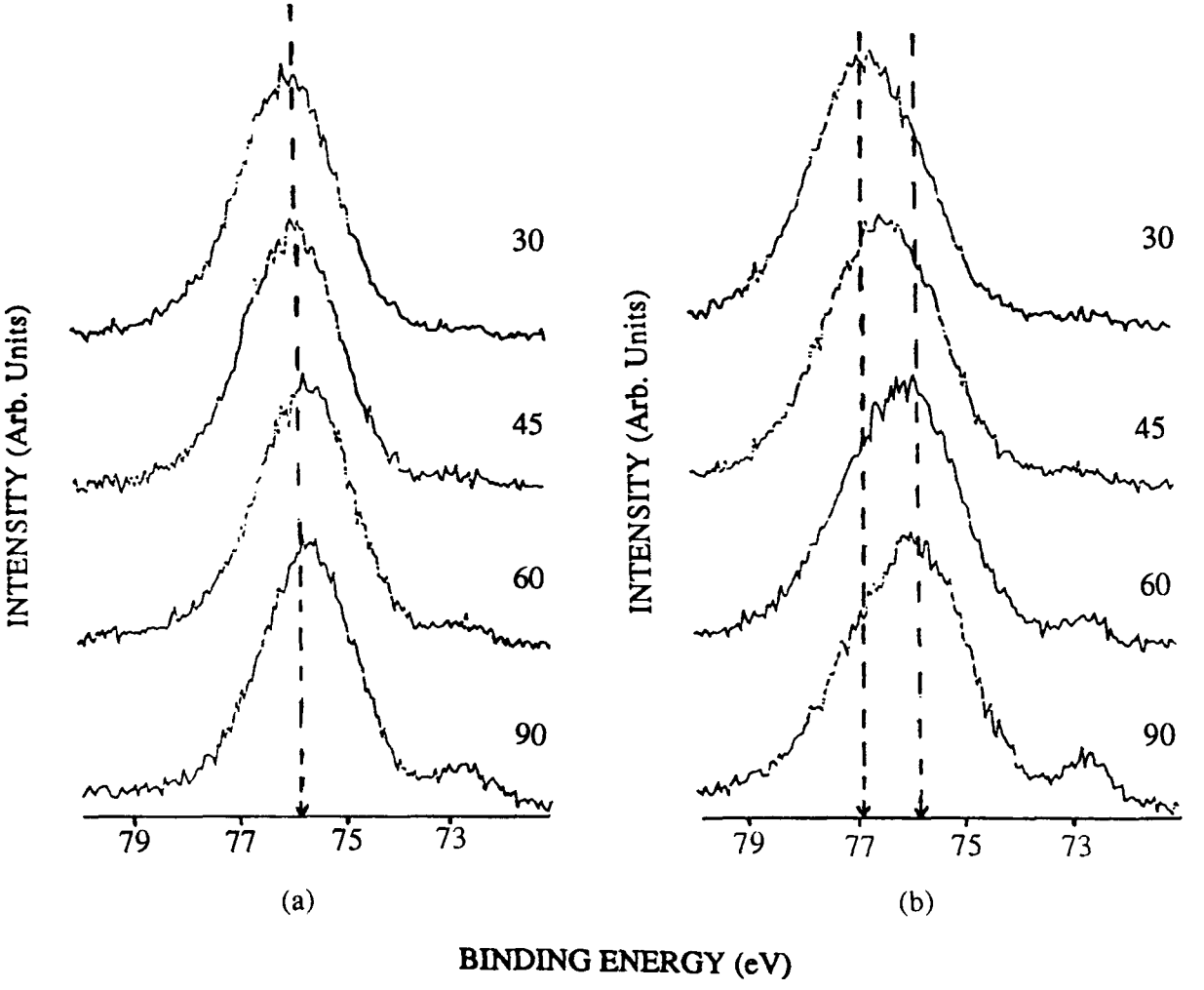

Figure 3.15 Al_{2p} spectra with varying take-off angles from 90^{o} to 30^{o} for (a) sample I (γ-MGPS/degreased Al interface) not biased and (b) sample I biased.

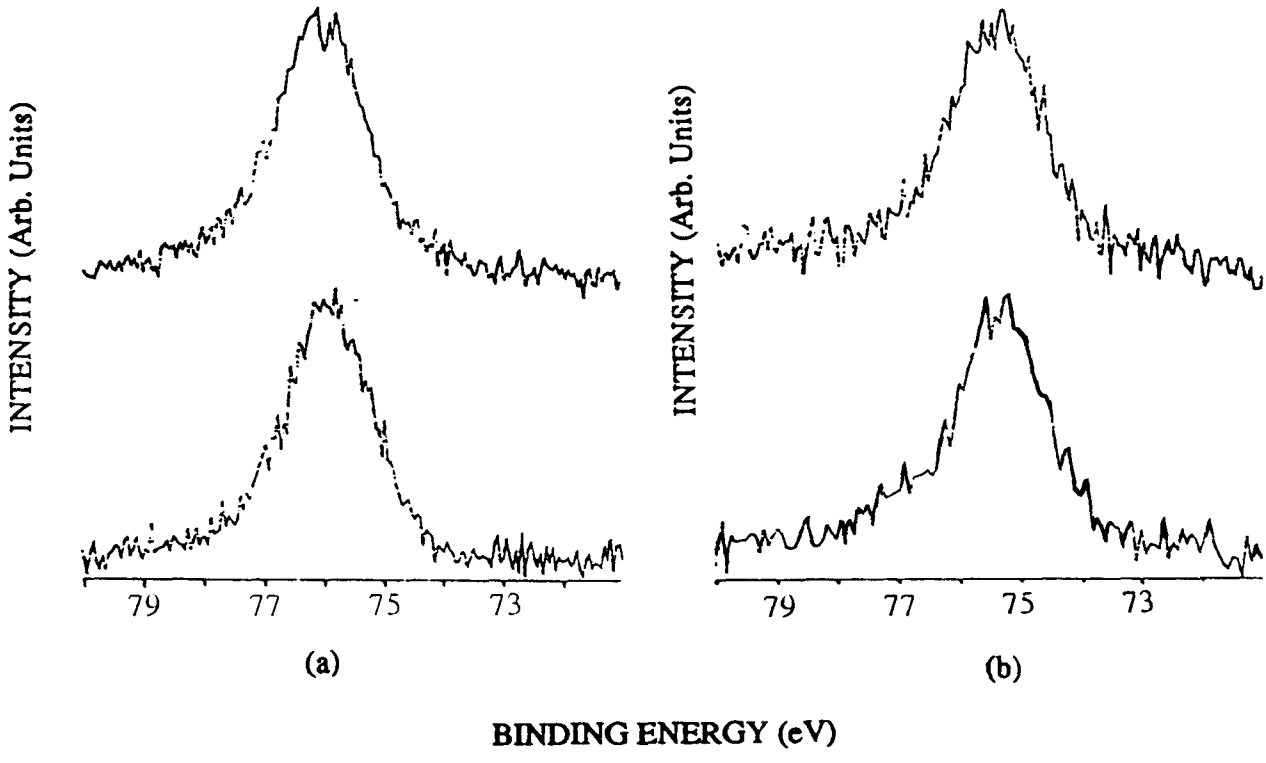

Figure 3.16 Al_{2p} spectra with varying take-off angles at 90^{o} for (a) sample G (γ-APS/degreased Al interfaces at pH=3.0) and (b) sample H (γ-APS/degreased Al interfaces at pH=10.4). Upper spectra have no bias potential while the lower ones were measured with a bias potential.

Turning to γ-MGPS, Figure 3.15 represents its biased and non-biased Al_{2p} spectra. An additional component towards the higher binding energies was also found when the bias was applied. Again we may postulate an occurrence of Al-O-Si bonding in the γ-MGPS/AlO_x interface. In this case, the peak shape does not change so much as for γ-GPS, and that presumably reflects the presence of different organofunctional groups. The epoxy group on γ-GPS, and the mercapto group in γ-GPS, may change the electrical characteristics of the Al-O-Si bonding regions and thereby lead to different charging factors, f.

Figure 3.16 shows the biased and non-biased Al_{2p} spectra for samples G and H with the take-off angle at 90°. Both their biased Al_{2p} photoemission peaks have no obvious change. We suggest that no differential charge is created in the aluminum, and that Al-O-Si bonding is not present in either of these interfaces.

From the results obtained for the biased samples E and F, we get direct evidence that the details of surface treatment can have a great influence on the nature of the adhesion. The degreased aluminum (sample E) does not interact with γ-GPS whereas the acid etched aluminum (sample F) does. It is possible that the continuous carbon overlayer on sample E prohibits γ-GPS having any direct contact with the AlO_x. By contrast, the acid etched aluminum surface provides some carbon-free AlO_x regions; then the ≡Si-OH from the silane can interact directly with the Al-OH on the panel surface. Turning to the interfaces of G and H, although acid etched aluminum surfaces also provide carbon-free AlO_x regions, the structure of γ-APS prevents any interaction taking place. It appears that no Al-O-Si bonding is formed at the γ-APS/Al interfaces.

Chapter 4. Concluding Remarks and Future Work

A. Concluding Remarks

From our studies of silane/Al interfaces discussed above, support is first given to the view that surface treatment is important for adhesion. The chromic acid etched Al panel (sample B) really has a different surface nature from that of the degreased one (sample A). The treatment changes the morphology of the carbon layer as well as the oxide layer. More metallic Al is exposed after the etching; the carbon overlayer is no longer continuous and that provides carbon-free AlO_x regions with the chance to interact directly with the silanes. The results got from the new ADXPS/bias technique measurements of γ-GPS/degreased Al (sample E) and γ-GPS/etched Al (sample F) appear in support with the above view for the surface pretreated Al panel. The extra structure in the Al_{2p} photoemission peak, observed with the applied bias potential, is assigned for the first time as a component from Al-O-Si bonded AlO_x.

A similar extra component in the Al_{2p} peak was obtained when γ-MGPS was applied on the etched Al panel. Again, that suggests direct Al-O-Si bonding exists in the interface. However, with the same probing technique, there is no direct evidence for γ-APS to interact with the AlO_x in either the acidic medium (pH=3.0) or the alkaline medium (pH=10.4). This result appears consistent with their film structures (figure 3.10); in both cases the ≡Si-OH groups orient away from the aluminum surface, so inhibiting the formation of Al-O-Si bonds.

Overall, the new results obtained in our work are consistent with the report of Matienzo et al. in relation to corrosion resistance. We have evidence that γ-GPS and γ-MGPS form direct chemical bondings with the aluminum oxide; this should give good couplings for the epoxy polymer/Al joints and help resist corrosion. On the contrary, γ-

APS forms no direct bonding with the Al oxide, and the modified epoxy/Al joints do not have good corrosion resistance.

B. Future Work

The research study reported here represents an exploratory study concerned with the chemical bonding between silanes and real aluminum surfaces [4.1, 4.2], but future expansions are possible in several directions:

1. Quantitative assessments of the ADXPS/bias potential technique:

Here we provided suggestive evidence for direct Al-O-Si chemical bonding at some silane/Al interfaces, but follow up work is required to give independent assessments, for example by vibrational spectroscopy or static SIMS. Under reasonable assumptions, it may be possible to have quantitative studies for this Al-O-Si bonding, an aspect that will be valuable to assess the goodness of the adhesion.

2. Characterization of Al oxide overlayers:

A full picture of the morphology of an etched Al oxide surface is still needed, for example from electron microscopy. That could enable more insight into the physical properties of the interface, and its effect on strength of adhesion. Further, different surface pretreatments for the Al panel could be performed to help find out the effect of treatment on overlayer coatings.

3. Polymer overlayer characterization:

From the XPS data we know that silanes polymerize during deposition, although the degree of polymerization is not clear. With more polymerization, the silanes may form better water repellent overlayers which are good for anti-corrosion (see below). Other spectroscopies, IR or SIMS for instance, may help to obtain further information about the polymerization.

4. Anti-corrosion studies:

Suggestive evidence is presented here that deposited organosilanes can act as effective corrosion inhibitors, but XPS and corrosion resistance studies are needed on the same samples. Anti-corrosion studies appear as an important topic in applied surface science. But as well as studying adhesion, it is also important to consider some practical questions. Will these Al-O-Si bondings retain in moist situations? Can they resist aggressive species such as Cl^- ? Such questions will be considered in follow up work.

References

[1.1] L.B. Hunt, Gold Bulletin 11 (1978) 22.

[1.2] L.H. Lee, Ed., "Fundamentals of Adhesion" (Plenum, New York, 1991).

[1.3] L.H. Lee, Ed., "Adhesive Bonding" (Plenum, New York, 1991).

[1.4] D.M. Brewis and D. Briggs, Polymer, 22 (1981) 716.

[1.5] J.D. Miller and H. Ishida, in "Fundamental of Adhesion", edited by L.H. Lee, (Plenum, New York, 1991) p.297.

[1.6] P. Walker, in "Surface Coatings", edited by A.D. Wilson, J.W. Nicholson and H.J. Prosser, (Elsevier Science, New York, 1987) p.190.

[1.7] E.P. Plueddemann, "Silane Coupling Agents" (Plenum, New York, 1991).

[1.8] B. Arkles, Chemtech, 7 (1977) 766.

[1.9] W.L. Baun, Appl. Surf. Sci. 4 (1980) 291.

[1.10] H. Leidheiser, Jr. and P.D. Deck, Science 241 (1988) 1176.

[1.11] Plato, Timaeus, English Translation by R.D. Archer Hinds (McMillan and Co., London, 1988).

[1.12] E.P. Plueddemann, "Silane Coupling Agents" (Plenum, New York, 1991) p.1.

[1.13] E.P. Plueddemann, "Composite Materials, Vol. 6" (Academic, New York, 1974) p.173.

[1.14] D.J. Falconer, N. MacDonald, and P. Walker, Chem. Ind. July (1964) 1230.

[1.15] P. Walker, Off. Digest, 37 (1965) 1561.

[1.16] M.J. Collie, Ed., "Corrosion Inhibitors Development since 1980" (Park Ridge, New Jersey, 1983) p.182.

[1.17] Ref. [1.7] p.34.

[1.18] Ref. [1.7] p.31.

[1.19] H. Ishida and J.L. Koenig, J. Colloid Interf. Sci. 64 (1978) 565.

[1.20] M.R. Rosen, J. Coating Tech. 50 (1978) 70.

[1.21] C.H. Chiang and J.L. Koenig, J. Colloid Interf. Sci. 83 (1981) 361.

[1.22] F.J. Boerio, L. Armogan, and S.Y. Cheng, J. Colloid Interf. Sci. 73 (1980) 416.

[1.23] C.H. Chiang, H. Ishida, and J.L. Koerig, J. Colloid Interf. Sci 74 (1980)396.

[1.24] P. Herder, L. Vagnerg, and P. Stenius, J. Colloid Surf. 34 (1988/89) 117.

[1.25] M. Gettings and A.J. Kinloch, J. Mat. Sci. 12 (1977) 2511.

[1.26] F.J. Boerio and J.W. Williams, Appl. Surf. Sci. 19 (1981) 19.

[1.27] F.J. Boerio, C.A. Gosselin, R.G. Dillingham and H.W. Liu, J. Adhesion 13 (1981) 159.

[1.28] K.W. Allen and M.G. Stevens, J. Adhesion 14 (1982) 137.

[1.29] A. Benninghoven, Surf. Sci. 53 (1975) 596.

[1.30] J. Comyn, D.P. Oxley, R.G. Pritchard, and C.R. Werret, J. Adhesion 28 (1989) 171.

[1.31] J. Comyn, D.P. Oxley, R.G. Pritchard, C.R. Werret, and A.J. Kinloch, Int. J. Adhesion and Adhesives 9 (1989) 201.

[1.32] D.M. Brewis, J. Comyn, D.P. Oxley, R.G. Pritchard, S. Reynolds amd C.R. Werrett, and A.J. Kinloch, Surf. Interf. Anal. 6 (1984) 40.

[1.33] L. Matienzo, D.K. Shaffer, W.C. Moshier, and G.D. Davis, J. Mat. Sci. 21 (1986) 1601.

[1.34] W. Thiedman, F.C. Tolan, P.J. Pearce, and C.E.M. Morris, J. Adhesion 22 (1987) 197.

[1.35] S. Hofmann, Surf. Interf. Anal. 9 (1986) 3.

[1.36] D. Briggs and M.P. Seah, Ed. "Practical Surface Analysis - by Auger and X-ray Photoelectron Spectroscopy" (Wiley, New York, 1983).

[1.37] W. Heiland E. Taglauer, Surf. Sci 68 (1977) 96

[1.38] A.J. Pertsin and Y.M. Pashunin, Appl. Surf. Sci. 44 (1990) 171.

[2.1] H. Hertz, Annal. Phys. 31 (1887) 982.

[2.2] A. Einstein, Annal. Phys. 17 (1905) 132.

[2.3] H. Robinson and W.F. Rawlinson, Phil. Mag. 28 (1941) 277.

[2.4] K. Siegbahn, Science 217 (1982) 4555.

[2.5] C.R. Brundle and M.W. Roberts, Proc. Roy. Soc. A331 (1972) 383.

[2.6] T.A. Carlson, "Photoelectron and Auger Spectroscopy" (Plenum, New York, 1975).

[2.7] M. Cardona and L. Ley, Ed., " Photoemission in Solids I, General Principles" (Berlin, New York, 1978).

[2.8] J.D. Andrade, in "Surface and Interfacial Aspects of Biomedical Polymer", edited by J.D. Andrade (Plenum, New York, 1985) p.105.

[2.9] M.P. Seah and W.A. Dench, Surf. Inter. Anal. 1 (1979) 2.

[2.10] G.E. Muilerbery, Ed., "Handbook of X-ray Photoelectron Spectroscopy", (Perkin-Elmer, Minnesota, 1979) p.154.

[2.11] Ref [1.36] p.114.

[2.12] N.S. McIntyre, Ed. "Quantitative Surface Analysis of Materials", (ASTM, Phildaelphia, 1977).

[2.13] C.D. Wagner, Anal. Chem. 44 (1972) 1050.

[2.14] C.K. Jorgenson and H. Berthou, Anal. Chem. 47 (1975) 482.

[2.15] C.S. Fadley, Prog. Surf. Sci. 16 (1984) 275.

[2.16] B.D. Ratner, T.A. Horbett, D. Shuttleworth and H.R. Thomas, J. Colloid Interf. Sci. 83 (1981) 630.

[2.17] MAX 200 User Manual (Leybold, Köln, Germany)

[2.18] Ref [1.36] p.17.

[3.1] A.C. Moloney, in "Surface Analysis and Pretreatment of Plastics and Metal", edited by D.M. Brewis, (Applied Science, London, 1982) p.193.

[3.2] A.C. Moloney, in "Surface Analysis and Pretreatment of Plastics and Metal", edited by D.M. Brewis, (Applied Science, London, 1982) p.177.

[3.3] J.D. Venables, D.K. McNamara, J.M. Chen and T.S. Sun, Appl. Surf. Sci. 3 (1979) 88.

[3.4] J.M. Chen, T.S. Sun and J.D. Venables, Nat. SAMPE Symp. Exhib. 22 (1978) 25.

[3.5] G.D. Davis, J.S. Ahearn, L.J. Matienzo, and J.D. Venables, J. Mater. Sci. 20 (1985) 975.

[3.6] C.D. Wagner, D.E. Passoja, H.F. Hillery, T.G. Kinisky, H.A. Six, W.T. Jasen, and J.A. Taylor, J. Vac. Sci. Technol. 21 (1982) 933.

[3.7] R. Bailey and J.E. Castle, J. Mater. Sci. 12 (1977) 2049.

[3.8] J.A. Taylor, J. Vac. Sci. Technol. 20 (1982) 751.

[3.9] F.J. Boerio, C.A. Gosselin, J.W. Williams, R.G. Dillingham and J.M. Burkstrand, in "Molecular Characterization of Composite Interfaces", edited by H. Ishida and G. Kumar, (Plenum, New York, 1982) p.171.

[3.10] Ref [1.7] p.105.

[3.11] H.R. Anderson, J.F.M. Fowkes, and F.H. Hielschadr, J. Polym. Sci. 14 (1976) 879.

[3.12] N.H. Sung, A. Kaul, I. Chin, and C.S.P. Sung, Polym. Eng. Sci. 20 (1982) 637.

[3.13] P.R. Moses, L.M. Wier, J.C. Lennox, H.O. Finklea, J.R. Lenhard, and R.W. Murray, Anal. Chem. 50 (1978) 576.

[4.1] Y.L. Leung, M.Y. Zhou, P.C. Wong, K.A.R. Mitchell, and T. Foster, Appl. Surf. Sci. 59 (1992) 23.

[4.2] Y.L. Leung, Y.P. Yang, P.C. Wong, K.A.R. Mitchell, and T. Foster, in preparation.